Journal Pre-proof

Immuno-proteomic profiling reveals aberrant immune cell regulation in the airways of individuals with ongoing post-COVD-19 respiratory disease

Bavithra Vijayakumar, Karim Boustani, Patricia P. Ogger, Artemis Papadaki, James Tonkin, Christopher M. Orton, Poonam Ghai, Kornelija Suveizdyte, Richard J. Hewitt, Sujal R. Desai, Anand Devaraj, Robert J. Snelgrove, Philip L. Molyneaux, Justin L. Garner, James E. Peters, Pallav L. Shah, Clare M. Lloyd, James A. Harker

PII: S1074-7613(22)00046-2

DOI: https://doi.org/10.1016/j.immuni.2022.01.017

Reference: IMMUNI 4796

To appear in: *Immunity*

Received Date: 10 August 2021

Revised Date: 17 November 2021

Accepted Date: 21 January 2022

Please cite this article as: Vijayakumar, B., Boustani, K., Ogger, P.P., Papadaki, A., Tonkin, J., Orton, C.M., Ghai, P., Suveizdyte, K., Hewitt, R.J., Desai, S.R., Devaraj, A., Snelgrove, R.J., Molyneaux, P.L., Garner, J.L., Peters, J.E., Shah, P.L., Lloyd, C.M., Harker, J.A., Immuno-proteomic profiling reveals aberrant immune cell regulation in the airways of individuals with ongoing post-COVD-19 respiratory disease, *Immunity* (2022), doi: https://doi.org/10.1016/j.immuni.2022.01.017.

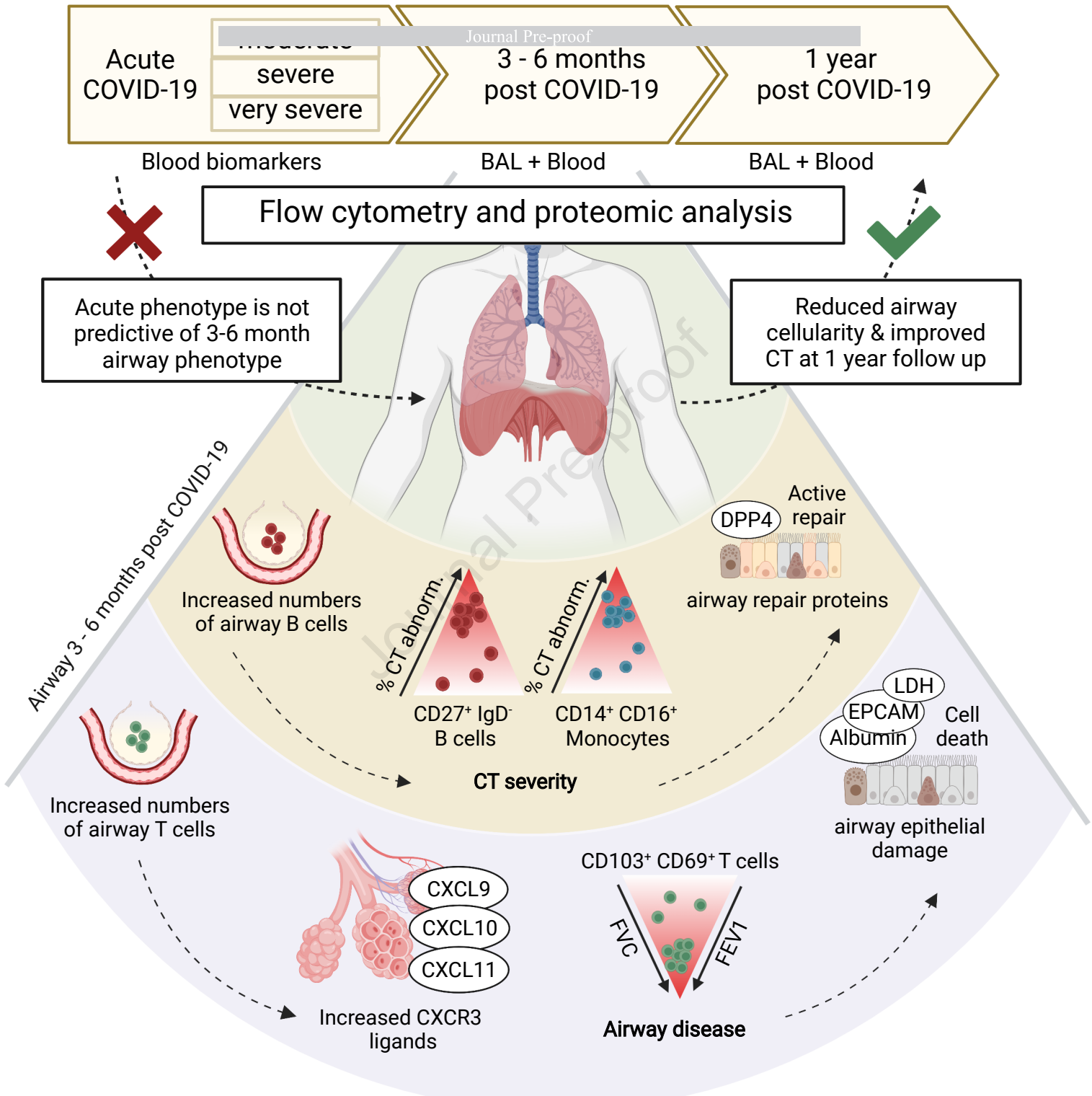

Title: Immuno-proteomic profiling reveals aberrant immune cell regulation in the airways of individuals with ongoing post-COVD-19 respiratory disease

Authors: Bavithra Vijayakumar[1,2,3,+], Karim Boustani[1,4,+], Patricia P. Ogger[1,+], Artemis Papadaki[5,+], James Tonkin[1,3], Christopher M. Orton[1,3], Poonam Ghai[1], Kornelija Suveizdyte[1], Richard J. Hewitt[1,3], Sujal R. Desai[1,3,6], Anand Devaraj[1,3], Robert J. Snelgrove[1,4], Philip L. Molyneaux[1,3], Justin L. Garner[2,3], James E. Peters[5,*], Pallav L. Shah[1,2,3,*], Clare M. Lloyd[1,4*] and James A. Harker[1,4,*]

[1]National Heart and Lung Institute, Imperial College London, London, UK
[2]Chelsea and Westminster Hospital, London, UK
[3]Royal Brompton and Harefield Hospitals, Guy's and St Thomas' NHS Foundation Trust, London, UK
[4]Asthma UK Centre for Allergic Mechanisms of Asthma
[5]Centre for Inflammatory Disease, Dept of Immunology and Inflammation, Imperial College London, London, UK
[6]Margaret Turner-Warwick Centre for Fibrosing Lung Diseases
[+]these authors contributed equally
*senior author

Lead contact: Dr James A Harker, j.harker@imperial.ac.uk
Sir Alexander Fleming Building, National Heart and Lung Institute, South Kensington Campus, Imperial College London, London, UK. SW7 2AZ.

Summary

Some patients hospitalized with acute COVID-19 suffer respiratory symptoms that persist for many months. We delineated the immune-proteomic landscape in the airway and peripheral blood of healthy controls and post-COVID-19 patients 3 to 6 months after hospital discharge. Post-COVID-19 patients showed abnormal airway (but not plasma) proteomes, with elevated concentration of proteins associated with apoptosis, tissue repair and epithelial injury versus healthy individuals. Increased numbers of cytotoxic lymphocytes were observed in individuals with greater airway dysfunction, while increased B cell numbers and altered monocyte subsets were associated with more widespread lung abnormalities. 1 year follow-up of some post-COVID-19 patients indicated that these abnormalities resolved over time. In summary, COVID-19 causes a prolonged change to the airway immune landscape in those with persistent lung disease, with evidence of cell death and tissue repair linked to ongoing activation of cytotoxic T cells.

Key words: respiratory viral infection, tissue resident memory, COVID19, SARS-CoV-2, airways

Introduction

Severe acute respiratory syndrome coronavirus 2 (SARS-CoV-2) related coronavirus disease (COVID19) manifests as a spectrum of acute illnesses ranging from mild respiratory symptoms to severe, sometimes fatal, respiratory failure (Docherty et al., 2020). While the acute impact of COVID19 on morbidity and mortality is well-documented, we are still in the infancy of understanding the longer-term consequences. Morbidity from a range of persistent symptoms, including breathlessness, fatigue and memory impairment have been noted in patients recovering after the acute illness and described under the umbrella term of "long COVID" (Nalbandian et al., 2021; Sigfrid et al., 2021). Complex respiratory complications have been found in up to 18.4% of inpatients (Drake et al., 2021), and persistent breathlessness reported in more than 50% of patients recovering from COVID19 (Mandal et al., 2021). The underlying aetiology for persistent respiratory morbidity is likely to be multifactorial but may be due to persistent parenchymal abnormalities and resultant ineffective gaseous exchange. Persistent radiological abnormalities post-COVID19 are common and may be present even up to 6 months post hospital discharge (Fabbri et al., 2021; Guler et al., 2021; Han et al., 2021; Myall et al., 2021). There is, therefore, a pressing need to understand the molecular and cellular basis of post-COVID19 pulmonary syndromes.

The acute immunological and inflammatory events that occur during human respiratory virus infections, including SARS-CoV-2, are relatively well described (Harker and Lloyd, 2021). In contrast, the immunological landscape of the human respiratory tract after recovery from acute viral infection is poorly understood. SARS-CoV-2 infection results in formation of long-lasting systemic immunological memory, with virus-specific antibodies and T cell responses still detectable in the majority of those infected at least 8 months post infection and higher titers seen in previously hospitalized individuals (Dan et al., 2021). Circulating lymphocyte counts and the function and frequency of monocytes are also reduced during acute disease, but they appear to return to normal shortly after resolution of acute disease (Mann et al., 2020; Scott et al., 2020). Likewise, plasma concentrations of inflammatory mediators such as IL-6 and CXCL10, that are highly elevated in acute disease, reduce as individuals recover (Rodriguez et al., 2020). Together, this suggests that systemic inflammatory and immune responses associated with acute disease severity resolve in line with recovery from the acute symptoms. It therefore remains unclear if the severity of inflammation during acute disease is associated with the persistent respiratory pathology seen in some SARS-

CoV-2 infected individuals months after infection, or if there is ongoing inflammation in these individuals.

This study examines the relationship between the immune system and respiratory pathology post-COVID19. The immune cell and proteomic composition of the airways and peripheral blood were analyzed in a group of previously hospitalized COVID19 patients with persistent radiological abnormalities in their lungs more than 3 months post discharge. In comparison to healthy individuals, the post-COVID19 airway showed substantial increases in activated tissue resident memory $CD8^+$ and $CD4^+$ tissue-resident memory (Trm) cells, and an altered monocyte pool. The airway proteome was also distinct from that observed in healthy individuals, with elevation in proteins associated with ongoing cell death, loss of barrier integrity and immune cell recruitment. None of these airway abnormalities were reflected in the proteome or immune cells of the matched peripheral blood. The scale of these alterations was not linked to the initial severity of disease while in hospital and were heterogenous; Some individuals displaying heightened T cell responses associated with significant increases in CXCR3 chemokines in the airways linked to prolonged epithelial damage and extracellular matrix (ECM) dysregulation, while other individuals exhibited a return to relative airway homeostasis. Subsequent long-term follow-up also suggested that these changes to the airway landscape progressively return to normal.

Results

Increased airway lymphocyte numbers characterize patients recovering from hospitalization with SARS-CoV-2

We recruited 38 patients undergoing bronchoscopy for investigation of persistent respiratory abnormalities 3-6 months following acute SARS-CoV-2 infection (post-COVID19) (**Figure 1).** All patients had ongoing respiratory symptoms and/or radiological pulmonary abnormalities on computed tomography (CT). Peripheral blood and bronchoalveolar lavage (BAL) was obtained. The post-COVID19 cohort was stratified based on the level of respiratory support used during their initial hospitalization with acute COVID19, into moderate (no/minimal oxygen administered), severe (non-invasive ventilation) and very severe (invasive ventilation). We used BAL fluid, plasma and historic flow cytometry analysis obtained from 29 healthy volunteers recruited prior to the COVID19 pandemic as controls (demographic information in **Table S1**).

We compared the cellular composition of BAL fluid in post-COVID19 patients to healthy controls (HC) by flow cytometry (Figure S1A). Post-COVID19 patients had significantly higher numbers of cells in their airways compared to the healthy controls (**Figure 2A**). This increased cellularity was due to elevated numbers of airway macrophages (AM), T and B cells **(Figure 2B)**. $CD56^{+}CD3^{-}$ (natural killer, NK) and $CD56^{+}CD3^{+}$ (NKT) cells, $CD14^{+}$ monocytes and eosinophils were similar to those in healthy controls, while neutrophils were decreased (**Figure 2B**). As a proportion of airway leukocytes, $CD14^{+}$ monocytes and neutrophils were decreased in post-COVID19 patients compared to controls (**Figure S1B**).

No association between the severity of acute COVID19 in hospital and the immune cell composition of the post-COVID19 BAL was observed (**Figure 2B**). In contrast to the peripheral lymphopenia that is associated with acute COVID19 (Chen and Wherry, 2020), we found that in this post-COVID19 patient cohort the frequency of T cells, B cells and $CD14^{+}$ monocytes in the peripheral blood was similar to healthy controls (**Figure S1C**), although the proportion of NK and NKT cells was decreased (**Figure S1C**). Collectively, these data indicate that after recovery from severe SARS-CoV-2 infection, immune cell frequencies in the peripheral blood are comparable to those in a group of age-matched controls. In contrast, the immune landscape of the airways remains altered, being marked by residual lymphocytes.

Post-COVID19 airways display a proteomic signature not reflected in blood.

We next evaluated the airway and blood (plasma) proteomes, using the Olink platform to measure 435 unique proteins in BAL and plasma from 19 post-COVID19 patients and 9 healthy controls. The proteins measured were highly enriched for immune-inflammatory processes (**Table S2A-C**). Principal component analysis (PCA) of BAL proteomes revealed differences between post-COVID19 patients and healthy controls (**Figure 3A**), with separation of case and controls most evident along PC1. In plasma, PCA also revealed differences, most evident along PC2, although the differences were less marked than for BAL. However, in both BAL and plasma there was considerable overlap in the spatial location of post-COVID19 and control in the PCA plots, indicating heterogeneity in post-COVID19 patients, with some displaying similar proteomic profiles to healthy controls. Unsupervised hierarchical clustering revealed two major clusters in BAL, one consisting predominantly of post-COVID19 samples and the other predominantly healthy controls (**Figure S2A**). In contrast, in plasma, there was no visible structure to the clustering and lack of clear separation of cases and controls (**Figure S2B**). These analyses indicates that the post-COVID19 phenotype is predominantly reflected by the airway proteome rather than the peripheral blood.

Differential protein abundance analysis comparing post-COVID19 cases with healthy controls identified 22 proteins in BAL with significantly altered concentration (5% false discovery rate, FDR) (**Figure 3B-C**, **Table S2D**). These were all upregulated in post-COVID19 patients compared to healthy controls (**Figure 3C**). To provide a succinct and standardised nomenclature, we report proteins by the symbols of the genes encoding them (see **Table S2A** for mapping to full protein names). The proteins that were most significantly differentially abundant between post-COVID19 and controls were: SERPINA7 (thyroxine binding globulin), DPP4 (dipeptidyl peptidase 4), SERPINA5 (plasma serine protease inhibitor), KLK6 (kallikrein related peptidase-6), LYVE1 (Lymphatic vessel endothelial hyaluronic acid receptor 1), AREG (amphiregulin), F3 (factor 3), FLT3LG (Fms-related tyrosine kinase 3 ligand), QPCT (glutaminyl-peptide cyclotransferase), MMP3 (metalloproteinase-3) and SRC (Proto-oncogene tyrosine-protein kinase Src) (**Figure 3C-D**). Pathway annotation of the 22 upregulated proteins using String-DB highlighted “leucocyte activation”, “regulation of cell death”, “response to injury” and “response to wounding” (**Table S2E).** Analysis of the relationship between the 22 differentially abundant proteins and the airway immune cell proportions showed that neutrophils most strongly correlated with AREG and LDLR (low density lipoprotein receptor), while monocyte proportions correlated with

F3, FLT3LG, MB (myoglobin) and IL1RN (IL-1 receptor antagonist protein) (**Figure 3E)**. Although elevated in the airways post-COVID19, T cells displayed only weak correlations with the differentially abundant proteins.

In contrast to BAL, no significant differences between protein levels were detected in plasma in post-COVID19 patients versus healthy controls (**Table S2F**). Comparison of the estimated $\log_2$ fold changes for the 22 proteins upregulated in post-COVID19 BAL fluid with the estimated $\log_2$ fold changes for these same proteins in plasma revealed no correlation (**Figure S2C-D**), indicating that the post-COVID19 airway proteomic signature is not reflected in the circulation.

The modest sample size and multiple testing burden of 435 proteins likely limited the statistical power to detect differentially abundant proteins. To examine whether there was evidence of signal in the proteomic data that was hidden by the hard-thresholding in the differential abundance analysis, we examined quantile-quantile (QQ) plots of the distribution of expected p-values under the null hypothesis of no proteomic differences between cases and controls versus the observed p-values. For both BAL and plasma, the QQ plots revealed substantial deviation from the diagonal (albeit more so in BAL), indicating the presence of systematic differences between post-COVID19 and healthy controls for plasma proteins as well as BAL proteins (**Figure S3A)**. Corroborating this, the distribution of p-values for the proteins was not uniformly distributed, with skewing towards zero (**Figure S3B**). This is consistent with separation of post-COVID19 and control samples on the PCA plots for both BAL and plasma. These data suggest that there are differences in both the BAL and plasma proteomes of post-COVID19 cases compared to healthy controls, but that the effects are much stronger in BAL.

To increase power, and investigate potential protein-protein relationships, we utilized a network analysis method, Weighted Coexpression Network Analysis (WGCNA) (Langfelder and Horvath, 2008; Zhang and Horvath, 2005), that leverages the correlation between proteins to enable dimension reduction, thus reducing multiple testing burden. We used WGCNA to identify modules of correlated proteins, and then tested for association between these protein modules (represented quantitatively by an eigenprotein value) and case/control status. In BAL, this revealed two modules (‘red’ and ‘blue’) significantly associated with case/control status (5% FDR) (**Table S2G-I**).

The red module consisted of 37 proteins (**Figure S4A, Table S2H**), characterized by proteins associated with chemotaxis, inflammation, cell death and repair. In post-COVID19 patients, we observed co-upregulation of groups of related red module proteins such as the CXCR3 chemokines (CXCL9, CXCL10 and CXCL11), and IL1A (interleukin-1A) and its antagonist IL1RN (**Figure S4A and B**). We used STRING-db to visualize known or predicted relationships between proteins in the module (**Figure S4A and B**). To highlight putative key proteins in the red and blue modules in a data-driven way, we identified hub proteins, defined as those that are highly interconnected in the proteomic network defined by WGCNA (**Table S2J**). This identified CASP3 (caspase-3), EPCAM (epithelial cell adhesion molecule), F3 and MB in the red module. F3 and MB, an oxygen binding protein release which is linked to muscle damage, were also identified as upregulated in the univariate differential abundance analysis (**Figure 3B-C**). CASP3 is involved in cell death, EPCAM and KRT19 (Keratin-19) are indicative of epithelial cell debris within the BAL, and TGFA (transforming growth factor A) is an EGFR ligand involved in epithelial repair. The presence of CASP3, EPCAM, KRT19 and TGFA in the red module therefore suggests that one of the key features of the post-COVID19 airway is the presence of ongoing epithelial injury and repair.

Blue module proteins were predominantly upregulated in post-COVID19 versus healthy control BAL (**Figure S5A**). The blue module was larger than the red module, containing 108 proteins involved in a wide range of biological activities. Several members were involved in cell adhesion and immune cell signaling. The hub proteins in the blue module were CD93 (Complement component C1q receptor), COMP (Cartilage oligomeric matrix protein), IGFBP3 (Insulin-like growth factor-binding protein 3), IL1R2 (Interleukin-1 receptor type 2), LYVE1, MMP2 (72 kDa type IV collagenase), NCAM1 (Neural cell adhesion molecule 1), SELL (L-selectin), TIE1 (Tyrosine-protein kinase receptor Tie-1), TNXB (Tenascin-X) and VASN (Vasorin) (**Figure S5B**). Of these, LYVE1 and VASN were also identified in the differential abundance analysis.

In contrast to the BAL network analysis, no protein modules in plasma were associated with case-control status. This suggests that persistent post-COVID19 respiratory abnormalities have a demonstrable proteomic signature in BAL that is distinct compared to that of healthy controls. In contrast, we were unable to detect changes in the plasma proteome of post-COVID19 patients, even with the enhanced statistical power provided by the WGCNA method.

There were no significant associations between the severity of initial infection and proteins in BAL fluid within the post-COVID19 cases, paralleling our flow cytometry

241 results. Thus, the immune-proteomic profile of the post-COVID19 airway does not
242 appear to relate to the severity of acute disease.
243
244 *CXCR3 ligands and markers of ongoing epithelial damage correlate with airway T*
245 *cell and monocyte responses*
246
247 Given that post-COVID19 patient airways displayed proteomic abnormalities and
248 elevated T, B and NK cells, we next sought to determine which BAL proteins were
249 associated with particular immune cell populations, and identified several significant
250 associations (5% FDR) (**Figure 4A and Table S2K**). The proportion of monocytes in
251 the airways was significantly associated with a range of airway proteins, including the
252 CCR7 ligand CCL19, the CXCR3 ligands CXCL9 and 11, TRAIL (TNFSF10), and
253 BAFF (TNFSF13B) (**Figure 4A**). CXCL9 and 11 also positively correlated with
254 lymphocyte and T cell frequencies and negatively correlated with airway macrophage
255 frequencies (**Figure 4A**). T cell frequencies positively correlated with SH2D1A (SLAM
256 associated protein or SAP). B, NK and NKT cells did not significantly correlate with any
257 protein.
258
259 In addition to displaying correlations with immune cell frequencies in the airways, the
260 chemokines CXCL9, 10 and 11, and their receptor, CXCR3, are all members of the
261 red WGCNA module that characterized the post-COVID19 airway. Given their shared
262 signaling pathway, we analyzed the contribution of these chemokines further by
263 calculating a composite score (reflecting an average fold change of each chemokine
264 relative to median concentrations found in HC BAL) and testing it for association with
265 BAL immune cell frequencies. This CXCR3 chemokine score strongly correlated with
266 airway T cell frequencies ($r = 0.68$, $p = 0.0001$), and with airway NK cells ($r = 0.62$, p
267 $= 0.001$). In contrast, there was no significant correlation to airway NKT cells ($p = 0.16$)
268 (**Figure 4B**). Within the post-COVID19 dataset (as CD16 was not present in historic
269 flow data used for healthy controls), total monocyte frequencies also correlated with
270 CXCR3 chemokine score ($r = 0.57$, $p = 0.016$) (**Figure 4C**). Intermediate
271 ($CD14^+CD16^+$) monocytes positively correlated with CXCR3 ligands, while $CD14^+$
272 monocytes displayed a negative correlation, and $CD16^+$ monocytes displayed no
273 correlation (**Figure 4C**). T cell proportions in the airways correlated tightly with the
274 concentration of CD8a protein, but not CD4, in the BAL (**Figure 4D**), suggesting the
275 increased airway T cells were most likely the result of increased $CD8^+$ T cell
276 frequencies.
277

We next determined the relationship between T cell frequencies and other protein members of the red module, specifically those indicating ongoing epithelial damage. CD8a correlated strongly with the concentrations of CASP3 and EPCAM, concomitant with two of the differentially expressed proteins: MB and DPP4 (**Figure 4E**). Collectively, these data suggest that proteins linked to the recruitment of T cells, especially cytotoxic T cells, are strongly associated with proteins that are both indicative of ongoing epithelial damage and upregulated in the airways post-COVID19.

To further evaluate this, we measured BAL CXCL9, -10 and -11 via cytometric bead immune assay in an expanded cohort of healthy controls (n = 29) and post-COVID19 patients (n = 38), including those samples on which Olink data was generated plus additional samples. Analysis of this larger sample set revealed that CXCL10 and CXCL11, but not CXCL9, were significantly upregulated in post-COVID19 compared to healthy control BAL (**Figure 4F**). We also confirmed the presence of increased damage in the post-COVID19 airway by measuring DPP4 and two markers of damage not analyzed by Olink, albumin and lactate dehydrogenase (LDH) (**Figure 4G**). DPP4, albumin and LDH were significantly upregulated in the airways of patients post-COVID19 compared to healthy controls, validating the observations made by Olink and confirming the presence of ongoing damage within the respiratory tract in patients previously hospitalized for COVID19.

Different airway immune populations associate with distinct aspects of post-COVID19 pathophysiology

The cause of persistent respiratory symptoms post-COVID19, and relationship to local changes in the immune response, is critical to the understanding and treatment of post-COVID19 respiratory disease. Therefore, we evaluated the relationship between the immune response and clinical measures of respiratory health taken shortly before bronchoscopy. Respiratory health was assessed through imaging (CT) and pulmonary function testing, including measurement of forced expiratory volume (FEV1, the amount of air a person can force out of their lungs in 1 second), forced vital capacity (FVC, the total amount of air an individual can exhale from their lungs), and gas transfer capacity of the lungs, measured by uptake of carbon monoxide (TLCO). There was heterogeneity within the cohort (**Table S1**). Pulmonary function and CT imaging were generally poorly correlated, aside from FEV1 and FVC which given their shared relationship, tightly correlated. In particular, the degree of CT abnormality only very

weakly correlated with reduced airway function (FEV1 or FVC) and gas transfer (TLCO) (**Figure 5A**).

To determine if this heterogeneity in respiratory function post-COVID19 was differentially associated with distinct immune cell phenotypes in the airways, we utilized high-parameter spectral deconvolution cytometry to analyze expression of 33 markers on BAL immune cells. Unbiased clustering of lymphocytes and myeloid cells using FlowSOM in parallel to manual gating (Figure S6A) indicated this approach could identify the majority of expected immune cell populations and subsets, while the absence of clusters of cells with unexpected marker expression patterns suggests the post-COVID19 airway does not feature substantial unique immune cell types (**Figure S6B and C**). Manual gating supported this, with enrichment of tissue resident immune cells in the BAL, and naïve lymphocyte populations in the blood of patients (**Figure S6D and E**). The proportions of immune cells and their subsets in the BAL revealed that no one immune cell type was dominantly linked to post-COVID19 respiratory pathophysiology (**Figure 5A**). Instead, different immune cell populations correlated with distinct indicators of disease. Neutrophils, $CD14^{+}CD16^{+}$ intermediate monocytes, and $IgD^{-}CD27^{+}$ memory B cells correlated most strongly with increased CT abnormality. Reduction in predicted FEV1 or FVC meanwhile were correlated more strongly with lymphocytes, with NKT, B and activated CD8 T cells having the strongest correlation with these measures of airway function. These correlations were not significant after a 5% FDR cut-off across the multiple tests was applied. Similar analysis using BAL cell number however supported these specific immune and clinical traits to be significantly correlated with a 5% FDR cut-off (**Figure S7**).

Segregating the cohort based on clinical measurements supported the observation that increases in different BAL biomarkers and immune cell populations are linked to distinct clinical features. BAL DPP4, LDH and albumin concentrations were not different in individuals with increased CT abnormality compared to those with more limited changes (**Figure 5B**). Albumin and LDH, but not DPP4, were increased in individuals with reduced FVC, while DPP4, but not albumin nor LDH, was increased in individuals with reduced TCLO (**Figure 5B**). Elevated BAL neutrophils correlated with more severe abnormalities on CT, FVC and TLCO (**Figure 5C**). BAL B cells were increased in individuals with enhanced CT abnormalities, or decreased FVC but not TCLO (**Figure 5C**). NK cells were increased in those with increased CT abnormality (**Figure 5C**). Total myeloid cells in the airways did not associate with any specific measure of respiratory disease. However, intermediate $CD16^{+}CD14^{+}$ monocytes were

increased in individuals with higher proportions of CT abnormality, while non-classical CD16^{+} monocytes were increased in individuals with reduced FVC (**Figure 5D**). Concomitant with enhanced BAL neutrophilia, the major neutrophil chemokine CXCL8 was increased in post-COVID19 compared to HC BAL, and CXCL8 concentration significantly correlated with airway neutrophils (**Figure 5E**). Similarly CCL2 was significantly increased in post-COVID19 BAL, and tightly correlated to BAL monocyte numbers (**Figure 5G**). CXCL8 or CCL2 did not segregate with worsened CT, FVC or TLCO (**Figure 5G and H**).

Collectively, these data highlight clinical assessments that measure distinct pathophysiological aspects of respiratory disease and are linked to different immunological components. CT abnormalities specifically were associated with granulocytic and monocytic involvement, whose presence is associated with chemokines canonical for their recruitment.

BAL T cell and B cells display discrete relationships with ongoing respiratory disease post-COVID19

We next carried out further correlation with the 3 biomarkers; DPP4 (the most differentially regulated protein in the post-COVID19 BAL), and LDH and albumin, as markers of ongoing damage in the airways. LDH activity inversely correlated with predicted FEV1 and FVC, and strongly correlated with proportions of various subsets of CD8 T cells in the BAL, with albumin showing similar, albeit weaker, links (**Figure 6A**). Conversely DPP4 was correlated with increased CT abnormality and reduced TCLO, but negatively correlated with the proportion of T cells in the BAL. Instead, the proportion of B cells, specifically memory B cells, were the only immune cell analyzed to show a strong correlation to DPP4 concentrations (**Figure 6A**).

B and T cells can play a critical role both in protective and pathological immune responses during acute COVID19 (Harker and Lloyd, 2021), and were significantly elevated in the BAL of individuals post-COVID19 compared to healthy controls (**Figure 2B**). Correlation with clinical measurements of respiratory function and pathophysiology suggested T cells were more strongly linked to airways disease, indicated by reduced FEV1 and FVC, while B cells, specifically memory B cells appeared to be linked to the full range of more severe pathophysiological changes seen post-COVID19 (**Figure 5A**). The number of CD69^{+} CD8 T and CD103^{+}CD69^{+} CD8 T cells in BAL was significantly increased among those post-COVID19 patients

with an FVC less than 90% of that predicted (**Figure 6B and C**). No other T cell population or subset showed significance in individuals with reduced FVC, but similar trends were present for activated CD4 T cells (**Figure 6B and C**). Conversely, analysis of B cells revealed that individuals with increased CT abnormality or reduced FVC or TCLO had significantly increased memory B cells in their airways, while naïve B cells and plasmablasts were not different (**Figure 6D**).

To examine the role of B cells in ongoing respiratory dysfunction further, antibody responses were measured. While total IgA in the BAL was similar in healthy controls versus post-COVID19 patients, total IgG was significantly increased (**Figure 6E**). As would be expected post-COVID19 patients, despite samples having been taken pre-vaccination, also had detectable antibodies against the receptor binding domain (RBD) of SARS-CoV-2's spike protein, with IgA and IgG abundance in the BAL, and IgG in the plasma (**Figure 6E**). The total or virus specific antibody concentrations present post-COVID19 displayed minimal correlation with the proportion of B cell subsets found either in the BAL or systemically (**Figure 6F**). Instead, BAL virus-specific IgG was significantly increased in individuals with reduced FVC, but not in individuals with increased CT abnormalities or reduced TLCO (**Figure 6G**). In line with this, virus specific antibody correlated tightly with CD4 and CD8 T cells in the BAL (**Figure 6H**). There was a particular correlation with activated e.g. $PD1^+$ $CXCR5^-$ CD4 and CD8 T cells, rather than $CXCR5^+$ $PD1^+$ CD4 and CD8 T cells which are more canonically associated with B cell helper functions.

Collectively, these data suggests that heightened T cell frequencies, especially $CD8^+$ Trm cells, are associated with increased indicators of cell death and ongoing airways disease post-COVID19. The presence of memory B cells in the BAL meanwhile was linked to increased DPP4, but not LDH, and a range of pathophysiological outcomes post-COVID19.

The post-COVID19 airway immune cell infiltrates decline over time

A subset of our cohort, who initially became infected with SARS-CoV-2 in Spring 2020, were also clinically assessed at 1 year post discharge. In line with a larger study, which included individuals without clinical indications requiring a bronchoscopy of radiological changes post-COVID19 (Vijayakumar et al., 2021), substantial reduction in CT abnormality within the lungs were seen at 1 year post discharge, compared to 3-6

months (**Figure 7A**). Improvements were also seen in patients' predicted FVC and TLCO by 1 year post discharge (**Figure 7A**).

There was however some variation in the degree of improvement from post-COVID19 respiratory disease, and 3 of the patients examined at 1 year continued to have substantive lung CT abnormalities justifying a follow-up bronchoscopy (demographics presented in **Table S3**). The total number of BAL cells recovered was greatly reduced in all 3 patients between the initial bronchoscopy and the 1 year follow up bronchoscopy, comparable to healthy control airways (**Figure 7B**). Similarly, numbers of T, B, NK, and NKT cells along with neutrophils and AMs were reduced to nearly or within the normal range seen in the airways of healthy individuals (**Figure 7B**). Non-classical and intermediate monocytes were also reduced at 1 year post discharge, but classical monocytes increased (**Figure 7B**). In the 2 individuals with elevated lymphocytes the ratio of CD4 to CD8 T cells increased (**Figure 7C**). Moreover, the proportion of CD8, but not CD4, T cells trended to decrease, although the proportion of each that were of a Trm or activated ($CD69^{+}$) phenotype, remained similar between the 2 time points (**Figure 7D**). Memory B cell proportions, but not plasmablasts, also declined between 3-6 months and 1 year post discharge (**Figure 7E**). Fitting with a progressive recovery trajectory, airway DPP4 concentrations declined in the 2 patients with elevated concentrations at the first bronchoscopy (**Figure 7F**). Of note however LDH, which was low to non-detectable in all 3 patients at the first bronchoscopy, showed a trend to increase while albumin concentrations were unchanged, but also within the range of healthy controls at both time points (**Figure 7F**).

Collectively, our findings show ongoing changes to the immune and proteome landscape of the airways. Distinct immune-protein signatures associated with different pathophysiological changes in the post-COVID19 lung. These changes, and lung pathology, do however appear to resolve over the longer (> 1 year) term.

Discussion

Recovery from COVID19 may be complicated by long-lasting symptoms including breathlessness. Here we studied patients previously hospitalized with COVID19, revealing a persistent proteomic and immunological abnormalities in the airways, but not peripheral blood, many months after acute infection. While there is substantial heterogeneity between patients, we observed upregulation of proteins associated with ongoing cell death, epithelial damage and tissue repair in post-COVID19 airways. This correlated with the presence of increased numbers of activated tissue resident CD8 T cells. Preliminary evidence suggests this altered airway landscape does improve over the long term, with reductions in airway immune cell numbers 1 year post discharge.

The acute response to SARS-CoV-2 infection is characterized by widespread upregulation of circulating proteins including IFN pathway proteins, chemokines, cytotoxic proteins, and markers of epithelial damage (Arunachalam et al., 2020; Filbin et al., 2021; Gisby et al., 2021). More severe disease is associated with increased inflammatory proteins (e.g. IL-6, TNF, GM-CSF, IL-1RN and IL-18) (Arunachalam et al., 2020; Filbin et al., 2021; Thwaites et al., 2021). A similar pattern of upregulated proteins, especially chemokines like CXCL10 and cytokines such as IL-6, is seen in the airways during acute COVID19 (Liao et al., 2020; Saris et al., 2021; Szabo et al., 2021). 3-6 months after SARS-CoV-2 infection however, despite the presence of ongoing respiratory morbidity, the plasma proteins differentially expressed during acute disease appear to have returned to similar concentrations to those seen in healthy controls. Even data dimension reduction approaches such as WGCNA fail to highlight any significant associations between COVID19 infection and the plasma proteome months later.

In contrast, the post-COVID19 airways continue to display an abnormal proteome, with both distinct and shared features to that seen in acute disease. Proteins linked to inflammation feature less prominently than in acute COVID19, whereas upregulation of proteins involved in epithelial damage and repair (e.g. the EGFR ligand AREG and the epithelial marker KRT19) persist. MMP-3, which regulates the extracellular matrix (ECM), was also differentially upregulated in the post-COVID19 airway. MMP3 and AREG are both upregulated after influenza A virus (IAV) infection *in vivo* in mice, and *in vitro* in human fibroblasts and epithelial cells (Boyd et al., 2020); and both are linked to epithelial repair and fibrosis in the lungs (Morimoto et al., 2018; Yamashita et al., 2011).

Elevated LDH and albumin in the airways provide further evidence of ongoing cell death and damage to respiratory barrier integrity post-COVID19. This observation is reinforced by the upregulation of a module of correlated proteins in the post-COVID19 BAL whose individual members reflect epithelial damage (EPCAM, KRT19), cell death (CASP3) and epithelial repair (TGFA), but also suggest a connection between these processes and immune cell recruitment and survival (CXCL9-11, IL-7). Increased cell death within the airways correlates with the frequency of T cells, primarily CD8 Trm cells, and with heightened respiratory dysfunction. In mouse models of severe acute respiratory virus infection, CD8 T cells are known to act as a double-edged sword. Although the cytotoxic molecules and cytokines they release are essential for clearing virus, they can also cause tissue damage and immunopathology (reviewed in (Duan and Thomas, 2016; Schmidt and Varga, 2018)). While pre-existing virus specific CD8 Trm cells in the airways is thought to be protective against a re-encounter with the same virus (Jozwik et al., 2015; Wu et al., 2014) little is known about their role in long-term respiratory virus-related pathology, especially in humans. This is primarily due to the lack of relevant samples collected during the recovery period. Our post-COVID19 data support the concept that sustained activation of CD8 Trm cells in the airways, long after recovery from acute disease, contributes to ongoing damage to the respiratory epithelium, resulting in airway disease.

The mechanism underlying increased Trm cells in the airways is unclear, although several studies have reported virus specific CD8 T cells in lung tissue up to a year post-infection (Cheon et al., 2021; Grau-Exposito et al., 2021; Poon et al., 2021). While virus specific CD4 and CD8 T cells rapidly expand, and form Trm cells, following SARS-CoV-2 infection (Szabo et al., 2021), these cells rapidly contract after resolution of acute disease, with CD8 Trm cells declining more rapidly than CD4 Trm (Slutter et al., 2017). The lungs of mice previously experienced IAV infection more robustly maintain CD8 Trm cells compared to uninfected lungs however, showing that severe infection promotes a pro-Trm niche (Slutter et al., 2017). This fits with our observation that CD8 Trm cell numbers vary dependent on the proteins and extent of damage in the airways, and change longitudinally in the same individuals, while CD4 Trm cells remain relatively static. A number of factors may contribute to the heterogeneity of the CD8 Trm niche in the post-COVID19 airway. Firstly, while all our post-COVID19 samples were taken from patients who tested negative for SARS-CoV-2 by qPCR immediately prior to bronchoscopy, persistent antigen has been observed months after other respiratory infections such as IAV (Kim et al., 2010), and SARS-CoV-2 antigen

depots could drive ongoing cytotoxic activity and maintenance of CD8 Trm cells. Secondly, the persistence of lung resident Trm cells is reliant on the availability of local T cell survival signals such as IL-7 (Szabo et al., 2019) and the CXCR3 ligands (Slutter et al., 2013). Indeed IL-7 and the CXCR3 ligands are part of the protein network that is maintained in the post-COVID19 airway. Lastly there is some evidence for indicating the development of auto-immunity in some patients recently recovered from COVID19 (Lucas et al., 2020; Wang et al., 2020). It is likely that these different mechanisms collectively act to shape CD8 Trm cell responses, and other immune cells, in the post-COVID19 airway, and the scale and duration of ongoing epithelial damage and respiratory dysfunction observed.

B cell frequencies were more elevated in individuals with more widespread lung abnormalities and reduced gas exchange. During acute infection or after vaccination B cells are critical in the generation of protective virus-specific antibody. Virus-specific B cells can be detected in the lungs up to 6-months post SARS-CoV-2 infection (Poon et al., 2021) but represent a minority of the B cells present in the human lung. Increased frequencies of airway and lung B cells, similar to those seen in the post-COVID19 airway, are commonly seen in a range of respiratory diseases including COPD and interstitial lung diseases (ILD) (Desai et al., 2018; Polverino et al., 2016). B cell frequencies do not correlate with virus-specific antibody, which is more tightly linked to the T cell responses suggesting a common antigen specific driver that B cells are not dependent on. Precisely how B cells contribute to ongoing respiratory pathology post-COVID19 is unclear; they can produce both pro-inflammatory and regulatory factors, and disruption of regulatory B cell function has been shown to be associated with fibrotic lung disease (Asai et al., 2019). B cells can also promote tissue repair by inducing activation and migration of fibroblasts (Ali et al., 2021). Thus, in the post-COVID19 airway B cells may be directly promoting aberrant tissue repair.

Functional impairment of monocytes and DCs in the peripheral blood of acutely infected patients (Arunachalam et al., 2020; Laing et al., 2020; Mann et al., 2020), and hyperactivation of airway monocyte populations, are features of acute severe COVID19 (Liao et al., 2020; Szabo et al., 2021). In our post-COVID19 patients, peripheral blood monocyte had normalized and did not correlate with markers of pulmonary dysfunction, but BAL intermediate monocytes were increased in patients with greater CT abnormalities. In humans, following inflammatory insults, monocytes are recruited to the airways to differentiate into new AMs (Byrne et al., 2020). Severe viral infection can cause rapid depletion of the airway macrophage pool (Pribul et al.,

2008), and different subsets of monocytes contribute differentially to the replenishment of lung macrophages (Evren et al., 2021). Monocyte to macrophage transition is also more pronounced in chronic lung disease, with the newly generated monocyte-derived macrophages acting in a pro-fibrotic fashion (Misharin et al., 2017). Increases in intermediate monocytes may therefore be indicative of heightened monocyte differentiation into airway macrophages, the numbers of which are increased in the post-COVID19 airway compared to healthy controls. Amplification of this process may then contribute to ongoing repair within the lungs.

The progressive resolution of radiological abnormalities in the majority of post-COVID19 patients has been described (Han et al., 2021), and within our study even the 3 patients with persistent respiratory abnormalities show improved CT and reduced airway immune cell infiltration. This fits with the hypothesis that SARS-CoV-2 infection can result in organizing pneumonia, with subsequent changes reflecting ongoing epithelial damage and healing parenchyma rather than established fibrosis (Kory and Kanne, 2020). Moreover, the involvement of the immune response in different aspects of ongoing respiratory disease post-COVID19 suggests this recovery could be accelerated using immunomodulatory treatments.

Limitations of the study:

Our post-COVID19 data are generated on patients undergoing clinically indicated bronchoscopy because of persistent respiratory abnormalities. Whether our findings extend to individuals with no radiological abnormalities or respiratory symptoms post-COVID19 remains unknown. This selection bias also affects longitudinal sampling greater than 12 months post-COVID19, since the majority of patients initially sampled between 3-6 months post-COVID19 had shown sufficient improvement in respiratory pathology such that a follow-up bronchoscopy was not indicated.

Although we did not detect a plasma proteomic signature post-COVID19, our limited sample size is likely not powered to detect small differences in circulating proteins between post-COVID19 patients and healthy controls. Examination of p-values distribution suggests that differences may exist but will require much larger studies to reveal them. Regardless, the absence of any correlation between the differentially expressed proteins in the airways and their corresponding changes in the plasma points to the limited utility of peripheral blood as an indicator of the pathological lung processes. A limitation of the Olink platform used is that the proteins measured were

highly enriched for those involved in immuno-inflammatory processes, and thus we did not have an unbiased assessment of the entire proteome.

Finally, as with most studies, we were limited to sampling the airways post-infection and did not have paired pre-infection samples for intra-individual comparisons. It is possible therefore that some differences observed between healthy controls and post-COVID19 patients could reflect a pre-infection phenotype. Indeed, one of the most differentially expressed proteins in the airways, DPP4, is the binding receptor for another coronavirus MERS (Raj et al., 2013), and capable of mediating some SARS-CoV-2 binding (Li et al., 2020). Thus, it is conceivable that pre-existing upregulation of DPP4 increased susceptibility to post-COVID19 syndrome via increased viral entry (i.e. reverse causation), rather than DPP4 upregulation occurring in response to COVID19. However, the longitudinal reduction of DPP4, alongside reduced CT abnormalities and increased pulmonary function, argues against this hypothesis. More generally, the majority of proteins and markers upregulated are associated with ongoing lung pathology in other contexts (e.g. LDH), and are absent or only present at very low concentrations in the healthy airway, suggesting that their upregulation is more likely to be a consequence of COVID19 than a pre-disposing risk factor.

Funding

This work was supported by a Wellcome Trust Senior Fellowship 107059/Z/15/Z to CML. JAH is supported by a Rosetrees Seed Fund (A2172) and an Imperial College Healthcare NHS Trust BRC award (RDF04). PLM is an Action for Pulmonary Fibrosis Mike Bray Fellowship. BV is funded by the Joint Research Committee on behalf of CW+ and Westminster Medical School Research Trust. KB is funded by an Asthma UK PhD Studentship as part of the Asthma UK centre in allergic mechanisms of asthma (AUK-BC-2015-01). RJS is supported by a Wellcome Trust Senior Fellowship (209458/Z/17/Z). JEP is supported by a UKRI COVID19 Rapid Response Rolling Call (MR/V027638/1), the Imperial College London Community Jameel and the Imperial President's Excellence Fund, and a UKRI Innovation Fellowship at Health Data Research UK (MR/S004068/2).

Acknowledgements

We thank Jack Gisby for statistical and analytical advice, Simone Walker for technical assistance and the staff of South Kensington Flow Cytometry Facility at Imperial College London for assistance with flow cytometry. We also thank Dr Ryan Thwaites and Professor Peter Openshaw, Imperial College London, for pre-submission paper critique.

Author contributions:

Conceptualization, **BV**, **PLS**, **JEP, CML** and **JAH**. Methodology, **BV, KB, PPO, AP, JEP** and **JAH**. Software, **AP** and **JEP**. Investigation, **BV**, **KB, PPO, PG** and **KS**. **BV**. Resources, **JT**, **CO**, **JG**, **PLS, RJH** and **PLM** . Formal analysis, **BV, KB, PPO, AP, SRJ** and **AD**. Data curation**, BV, PPO** and **AP**. Visualization**, KB**, **PPO**, **AP** and **JAH**. Writing – Original draft,. **JAH**. Writing – Review & Editing, **BV**, **KB**, **PPO**, **AP**, **JEP**, **PLS** and **CML**. Supervision, **RJS, JEP, PLS, CML** and **JAH**. Project administration, **CML** and **JAH**. Funding acquisition, **PLS**, **CML** and **JAH**. For information on proteomics contact James E Peters, j.peters@imperial.ac.uk; For clinical information contact Pallav L Shah, pallav.shah@imperial.ac.uk; For epithelial cell biology and repair contact Clare M Lloyd, c.lloyd@imperial.ac.uk; For all other queries contact James A Harker, j.harker@imperial.ac.uk.

Figure legends

Figure 1: Schematic of techniques performed on airway and blood samples

Schematic showing samples collected from healthy control donors (recruited 2015 – 2019 pre COVID-19) and from COVID-19 patients. COVID-19 patients were recruited for this study if presenting with ongoing respiratory symptoms 3 months post hospital discharge and CT and LFT were performed. Bronchoscopy was performed when clinically indicative (n = 38). Peripheral blood for subsequent analysis was obtained at time of bronchoscopy. Blood biomarker tests were performed during hospitalisation and at the first follow-up visit. Immune cell profiling and proteome analysis was performed on airway (BAL) and peripheral blood (plasma) samples from healthy controls and post COVID-19 patients (3 – 6 months post hospitalisation) using traditional and spectral flow cytometry, Olink high-throughout proteomic assay and univariate protein analysis. Immune and proteome data was integrated with acute severity and blood biomarkers during hospitalisation and at first follow-up. Patients were followed-up to 12 months post-discharge. When clinically indicative a bronchoscopy was performed at this time point (n = 3). Immune cell and univariate protein analyses were performed on airway and peripheral blood (plasma) samples at this time point.

LFT = lung function test, BAL = bronchoalveolar lavage, CT = computed tomography scan

Figure 2: Immune cell profile is altered in post-COVID-19 BAL over 80 days after discharge

(A) Left: Total number of cells in BAL from healthy controls and post COVID-19 patients. Right: total number of cells in BAL from post-COVID19 patients, stratified according to severity of the acute illness. **(B)** Total cell numbers of immune populations ($x10^6$/ml) in BAL from healthy controls and post-COVID19 patients, based on gating shown in Methods Figure 1. **(A - B)** Data are presented as mean ± SEM. Healthy controls n = 16, post-COVID-19 patients n = 28, moderate n = 9, severe n = 11, very severe n = 8. Statistical significance was tested by Mann Whitney U test or One-Way ANOVA + Tukey's multiple comparison test. *P < 0.05, **P < 0.01, ***P < 0.005. See also Figure S1.

Figure 3: A distinct proteome is present in the post COVID-19 airway

436 proteins in BAL and plasma 435 proteins were measured using Olink immunoassays in post-COVID19 patients (n = 19) and healthy controls (n = 9). **(A)** Principal component analysis (PCA) of BAL and plasma proteomes: each point

represents a sample. **(B)** Left: heatmap displaying Z-score normalised protein abundance for the 22 proteins that were significantly differentially abundant (5% FDR) between post-COVID19 and healthy controls in BAL. Samples have been ordered by case control status and then by peak severity during acute COVID-19 infection. Proteins are ordered by hierarchical clustering. Right: heatmap for these same 22 proteins in plasma, presented in the same order as for BAL. **(C)** Volcano plot showing differentially protein abundance analysis between post-COVID19 patients and healthy controls in BAL. Nominal –log10 P values are shown. Significantly differentially abundant proteins (5% FDR) are coloured in red and labelled. **(D)** BAL and plasma normalised protein abundance (NPX) expression for the 5 most significantly differentially abundance proteins between post-COVID19 patients and healthy controls. PBH = Benjamini-Hochberg adjusted p-values. **(E)** Correlation between the 22 differentially abundant proteins (from the analysis of post-COVID19 versus HC) and immune cell frequency in BAL. See also Figure S2-5.

Figure 4. CXCR3 ligands and markers of epithelial damage correlate with CD8 T cells numbers in the airways

BAL immune cells and protein concentrations were analysed post-COVID19 infection. **(A)** Heatmap displaying the relationship between proteins and immune cell frequencies. The proteins and immune cell traits displayed are those with at least one significant (5% FDR) association from linear regression analyses (see **Supplementary File 1K**). **(B-C)** For each sample, protein concentrations for CXCL9, -10 and -11, were normalised to the median concentration in healthy controls. For each sample, the mean of the normalised values for the 3 proteins was calculated to provide a summary metric for CXCR3 chemokines. This was then plotted against versus **(B)** T, NK and NKT proportions in post-COVID19 patients and healthy controls and **(C)** monocyte frequencies and subsets in post-COVID19 patients only. **(D)** BAL T cell frequency versus CD4 and CD8a concentrations as measured by Olink. **(E)** CD8a concentration versus CASP3, EPCAM, MB and DPP4 in the airways. **(F)** CXCL9, 10 and 11 concentration in in the BAL were measure by legendplex. **(G)** DPP4, albumin and LDH concentrations in the BAL determined by ELISA. Data are presented as median ± IQR. **(A)** Pearsons correlation of n = 19 post-COVID19 patients, the r value is shown. **(B-E)** Each point represents an individual patient, linear regression line +/- 95% confidence intervals are depicted, and r and p values from Pearsons correlation are stated. **(F & G)** represents n = 38 post-COVID19 and n = 20 healthy control individuals. Statistics were conducted using Mann-Whitney U test. *P < 0.05, **P < 0.01, ***P < 0.005, ****P < 0.001. pCOVID = post-COVID19.

727

728 **Figure 5. Distinct airway proteomic and immune cell phenotypes correlate with**
729 **distinct indicators of respiratory pathology post COVID. (A)** Immune cell
730 proportions in the BAL, as a percentage of total leukocytes, BAL albumin (ug/ml), LDH
731 (OD450) and DPP4 (ng/ml) were correlated with CT (% abnormality) or FEV1, FVC
732 and TLCO (% of predicted normal). Spearman's rho is displayed as a heatmap. **(B)**
733 Albumin (ug/ml), LDH (OD450) and DPP4 (ng/ml) in the BAL segregated by CT
734 abnormality (%), predicted FVC (%) and predicted TLCO (%). **(C)** The number of major
735 immune cell population per ml of BAL versus CT abnormality, FVC and TLCO. **(D)**
736 Total number of monocyte subsets per ml BAL was segregated by CT, FVC and TCLO.
737 **(E)** BAL CXCL8 (pg/ml) measured by Legendplex in HC and post COVID-19 patients
738 and correlated versus total neutrophil numbers (per ml/BAL). **(F)** BAL CXCL8 (pg/ml)
739 measured by legendplex in post COVID-19 patients segregated by CT abnormality
740 (%), predicted FVC (%) and predicted TLCO (%). **(G)** BAL CCL2 (pg/ml) measured by
741 legendplex in HC and post COVID-19 patients and correlated versus myeloid cells
742 ($CD11b^+$) in the BAL. **(H)** BAL CCL2 (pg/ml) measured by legendplex in post COVID-
743 19 patients segregated by CT abnormality (%), predicted FVC (%) and predicted TLCO
744 (%). Where applicable individual points are shown, and data are presented as median
745 ± IQR. Each point represents an individual patient. Statistical significance for **(B-H)**
746 was tested by Mann-Whitney U test. Benjamini-Hochberg adjusted (5% FDR) p-values
747 *P < 0.05, **P < 0.01, ***P < 0.005, ****P < 0.001. Pearson's correlations were
748 performed in E and G, r and p values are shown, as is a line of best fit +/- 95%
749 confidence intervals. See Figure S6 and 7.

750 **Figure 6. Increased airway T cell and B cell abundance is associated with more**
751 **severe ongoing respiratory pathophysiology post COVID-19. (A)** Immune cell
752 proportions in the BAL, as a percentage of total leukocytes, BAL albumin (ug/ml), LDH
753 (OD450) and DPP4 (ng/ml) were correlated with BAL albumin, LDH and DPP4
754 concentrations. **(B)** BAL T cell subtypes and **(C)** subsets of CD4 and CD8 T cells were
755 analyzed against FVC. **(D)** B cells subsets numbers per ml BAL segregated by CT,
756 FVC and TLCO. **(E)** Total and RBD specific IgA and IgG were measured in the BAL
757 and plasma. **(F)** Antibody concentrations were correlated with BAL and plasma B cell
758 subsets of total leukocytes. **(G)** Antibody concentrations measured in BAL and plasma
759 segregated by CT, FVC and TLCO. **(H)** Antibody concentrations were correlated with
760 BAL CD4 and CD8 T cells and their subsets as a proportion of total leukocytes. (**A, F**
761 **& H**) Spearman correlation. Correlations p < 0.05 after Benjamini-Hochberg

adjustment for an FDR of 5% are indicated by thickened boxes. **(B-E, G)** was tested by Mann-Whitney U test. Benjamini-Hochberg adjusted (5% FDR) *P < 0.05, **P < 0.01, ***P < 0.005, ****P < 0.001. A, F & G are display spearman's rho correlation.

Figure 7. Reduced cellularity is observed in the airways one year after initial bronchoscopy post-COVID19. (A) % lung CT abnormality or predicted FVC (%) or TLCO (%) at first appointment and 1 year follow up (n = 17 pCOVID19 patients). **(B)** Total cell counts and cell counts of lymphocyte populations, macrophages, neutrophils and monocyte subsets in the BAL. **(C)** Proportions of T cell subsets and **(D)** CD4 and CD8 $CD69^+$ $CD103^+$ as a proportion of BAL T cells **(E)** Proportions of memory ($CD27^+IgD^-$) and plasmablasts ($CD27^+CD38^+$) of $CD20^+$ B cells in the BAL. **(F)** DPP4, LDH and albumin measurements in BAL. All data depict first bronchoscopy between 3-6 months post discharge and at one year post discharge. Each point represents a single patient. (B-E) represent n = 3 patients. Green shading indicates median+/-IQR for proportions of populations and mediator concentration observed in healthy airways. (A) Wilcoxon matched-pair signed rank test. * p <0 .05, *** p < 0.001

Resource Availability

Lead Contact

Further information and requests for resources and reagents should be directed to and will be fulfilled by lead author James A. Harker (j.harker@imperial.ac.uk).

Materials availability

This study did not generate new unique reagents.

Data and code availability

Proteomic data has been deposited in the Dryad repository and are publicly available as of the date of publication. Accession numbers are listed in the key resource table. All original code has been deposited at Zenodo and is publicly available as of the date of publication. Additional Supplemental Items (Table S2) are available from Mendeley Data at http://dx.doi.org/10.17632/th35tt4zwm.1. All DOIs are listed in the key resource table.

Experimental model and subject details

Human samples

Post-COVID19 bronchoalveolar lavage fluid (BAL) was obtained from patients recruited to the PHENOTYPE study (NCT 04459351), an observational, longitudinal study recruiting patients at Chelsea and Westminster Hospital, London. 38 samples were collected from patients requiring sampling for clinical purposes. Ethical approval for the study was given by Yorkshire & The Humber - Sheffield Research Ethics Committee (IRAS 284497).

Patients who met the inclusion and exclusion criteria were recruited to the PHENOTYPE study (demographics in Table S1):

Inclusion criteria for the study were:

- Aged 18 years or older
- Previous confirmed COVID-19 infection (positive PCR or antibody)
- Attending a respiratory follow-up outpatient appointment for follow-up of persistent respiratory symptoms following visit post hospital attendance with COVID-19. infection or referred by the community for covid-related symptoms.

Patients were seen at approximately 4-6 weeks (Visit 1) and 3 months (Visit 2) following discharge from hospital or referral (if referred from the community). Patients underwent clinical assessment at both visits, including collection of demographic data, clinical history and clinical examination and assessment of vital parameters (heart rate, peripheral oxygen saturations, blood pressure reading and temperature). They also underwent clinical blood tests (including full blood count, renal function, liver function, C-reactive protein (CRP), ferritin, fibrinogen, D-dimer and pro-calcitonin). Patients had a computed tomography (CT) scan of the lungs approximately 3 months post discharge from hospital. In patients with abnormal CT findings, or persistent respiratory symptoms, a bronchoscopy and lavage was performed as part of clinical work-up. Bronchoscopy was performed under conscious or deep sedation. 150 ml of normal saline were instilled into the most affected segment (as determined by CT imaging), in 50 ml aliquots. 10 ml of fluid return was used for the scientific analysis described in this paper. Patients underwent formal lung function tests (including spirometry, lung volumes and gas transfer) near the time of the bronchoscopy (usually during the days immediately preceding the procedure). Lung function testing was performed in accordance with the American Thoracic Society and European Respiratory Society guidelines (2019). Further follow-up was determined on the basis of clinical need, with a maximum follow up period of up to 2 years post hospital discharge or referral.

Control, uninfected bronchoalveolar lavage was obtained from healthy donors (collected between April 2016 and December 2019). Ethical approval for the study was granted by the Research Ethics Committee (15/SC/0101) and all patients provided informed written consent as described previously (Allden et al., 2019; Byrne et al., 2020; Invernizzi et al., 2021). Briefly, 240 ml aliquots of warmed sterile saline were instilled in the right middle lung and aspirated by syringe. Lavage aliquots were pooled for each subject. All subjects provided written, informed consent to participate in the study. Healthy volunteers had no self-reported history of lung disease, an absence of infection within the last 6 months and normal spirometry.

Method details

Scoring of Computed Tomography scans

All CT scans were reviewed by two Thoracic Radiologists (AD and SRD), who have over 20 years' experience, and were blinded to the clinical data. CT scans were scored by consensus and the overall extent of opacified lung quantified to the nearest 5%.

848

849 **Processing of airway bronchoalveolar lavage samples**

850 BAL samples were processed and stained on the day of sample collection. BAL was
851 strained through a 70μm filter and subsequently centrifuged (1800 rpm, 2 min, 4°C).
852 Supernatant was snap-frozen and stored at -80°C. Pellets were incubated in red blood
853 cell lysis buffer (155mM NH_4Cl, 10mM $KHCO_3$, 0.1mM ethylenediaminetetraacetic
854 acid, pH 7.4) for 10 minutes before washing and resuspension in complete media
855 (RPMI 1640 with 10% fetal calf serum, 2mM L-glutamine, 100U/ml penicillin-
856 streptomycin).

857

858 **Processing of blood samples**

859 Peripheral blood was collected in EDTA coated vacutainers on the same day as
860 bronchoscopy. 1ml blood was centrifuged at 100g for 10 minutes (4°C), followed by
861 centrifugation at 20,000g for 20 minutes (4°C) to separate plasma, which was
862 subsequently stored at -80°C. 2ml blood from post COVID-19 patients was incubated
863 with red blood cell lysis buffer (155mM NH_4Cl, 10mM $KHCO_3$, 0.1mM
864 ethylenediaminetetraacetic acid, pH 7.4) for 10 minutes before washing and
865 resuspension in complete media (RPMI 1640 with 10% fetal calf serum, 2mM L-
866 glutamine, 100U/ml penicillin-streptomycin). 2.5 ml blood from healthy controls was
867 used to isolate peripheral blood mononuclear cells (PBMC) by Percoll density
868 centrifugation, as per manufacturer's instructions.

869

870 **Flow cytometry staining**

871 For traditional flow cytometry, 2 - 5 $x10^5$ cells were plated, while for high parameter
872 analysis using the Cytek Aurora 1 x 10^6 cells from each site were used. Cells were
873 washed with PBS and incubated with either near-infrared (traditional flow cytometry)
874 or blue (Cytek Aurora) fixable live/dead stain (Life Technologies), as per the
875 manufacturer's instructions. Before incubation with human fc block (BD Pharmingen)
876 cells were washed with FACS buffer (1% FCS, 2.5% HEPES, 1mM EDTA) and surface
877 staining was performed at 4°C for 30 minutes using antibody panels as described in
878 the **Key Resources Table**. Surface staining was followed by washing with FACS
879 buffer and fixation with 1% paraformaldehyde for 10 minutes. Labelled cells were
880 acquired on a 4-laser BD Fortessa (traditional flow cytometry; BD Bioscience) or 5-
881 laser Cytek Aurora flow cytometer (Cytek Bio).

882

883 **Flow cytometry analysis**

Conventional flow cytometry data was analysed using FlowJo v 10.6 (Tree Star). Data was pre-gated to exclude doublets and dead cells. In BAL samples $CD45^+$ cells were selected, and immune cell populations were identified using the gating strategy shown in **Figure S1A**. Percentages of the $CD45^+$ gate were calculated. In blood samples, leukocytes were selected based on FSC and SSC and immune cell populations were identified using the gating strategy shown in **Figure S1A**. Percentages of total leukocytes were calculated. High-parameter spectral deconvolution flow cytometry data from the Cytek Aurora was analysed using Cytobank (Beckman). tSNE analysis was performed on 300,000 events from 11 files. Iteration number was set to 1500 with a perplexity of 30 and theta of 0.5. FlowSOM analysis was performed subsequently using hierarchical consensus clustering with 12 metaclusters, 100 clusters and 10 iterations. Manual gating of high parameter cytometry data was carried out as shown in **Figure S6A**. Heatmaps were generated from median fluorescence values in Prism 9.0 (GraphPad).

Olink proximity extension proteomic assay

Plasma and BAL proteomic measurement was performed using the Olink proximity extension immunoassay platform. Five 92-protein multiplex Olink panels were used ('Inflammation', 'Immune Response', 'Cardiometabolic', Cardiovascular 2', 'Cardiovascular 3'), providing measurements of 460 protein targets per sample. Cryopreserved BAL and plasma samples were thawed on ice and mixed well by pipetting before plating 88 samples per plate ensuring case/control balance and random well ordering to prevent confounding of technical and biological effects. For BAL samples, a pilot study was performed using three control samples and three post-COVID19 samples (severe group) to determine optimal dilution parameters. Ultimately BAL was used neat. Since a small number of proteins were assayed on more than one panel, we measured a total of 435 proteins. We removed duplicate assays at random prior to subsequent analyses.

CXCR3 chemokine composite score

To create a composite score that reflected the CXCR3 chemokines (CXCL9, CXCL10 and CXCL11), we used the following approach. For each sample, protein concentration for CXCL9, -10 and -11, were normalised to the median concentration in healthy controls (to avoid unduly weighting the score towards chemokines with higher NPX values). For each sample, the mean of the normalised values for the 3 proteins was then calculated to provide a summary metric for CXCR3 chemokines.

Epithelial damage marker analysis in BAL

DPP4 (R&D systems, DY1180) and albumin (Bethyl Laboratories, E80-129) concentrations in the BAL were quantified by ELISA according to manufacturer's instructions. LDH concentrations were quantified using an *in vitro* toxicology assay (Sigma, TOX7). Briefly, 25μl of BAL sample were incubated with 50μl of LDH assay reaction mixture. After 30 minutes, the reaction was stopped with 7.5μl 1N HCL and absorbance was measured at 490nm with background correction at 690nm. All absorbances were measured using a SpectraMax i3x (Molecular Devices).

Total antibody measurement in BAL

Total antibody concentrations were measured in BAL by ELISA according to manufacturer's instructions (ThermoFisher Scientific, 88-50550-88, 88-50600-88). Briefly, plates were coated overnight with anti-IgG or –IgA capture antibody. BAL samples were added to plate at a dilution of 1:500 for IgG and 1:100 for IgA and incubated for 2 hours at room temperature. Plates were next incubated with detection antibody for 1 hour at room temperature and developed with TMB substrate. Absorbances at 450nm were measured using a SpectraMax 3i plate reader (Molecular Devices, USA)

SARS-CoV-2 RBD-specific antibody measurement

ELISAs against RBD-specific IgG and IgA were developed in-house using recombinant SARS-CoV-2 spike RBD protein (Sino Biologicals Inc., 40592-VNAH). Plates were coated overnight with 1μg/ml of protein and BAL and plasma samples were serially diluted from neat and 1:20, respectively, and incubated at room temperature for 2 hours. Pooled plasma samples from positive controls were added to each plate to allow for normalisation. Plates were incubated with goat anti-human IgG/IgA-HRP (Southern Biotech, 2040-05/2050-05) for 1 hour at room temperature. Plates were developed with TMB substrate (Neogen, 308177) and reactions stopped with 0.18M sulfuric acid before measurement of absorbance at 450nm using a SpectraMax 3i plate reader (Molecular Devices, USA).

Pro-inflammatory chemokine analysis in BAL

13 pro-inflammatory chemokines were measured in BAL using a LEGENDplex bead-based assay according to manufacturer's instructions (Biolegend, 740984). Briefly, 25μl of neat BAL sample was added to 25μl assay buffer. Beads were added to each well and incubated on a shaker at 800rpm for 2 hours at room temperature. Plates

were centrifuged and washed before addition of detection antibody. Plates were incubated with detection antibody for 30 minutes on a shaker at 800rpm. Plates were washed and samples were acquired using a BD Fortessa flow cytometer (BD Biosciences, USA). Data were analysed using the LEGENDplex data analysis software (Biolegend).

Quantification and statistical analysis

Olink proximity extension proteomic analyses

Proteomic data was normalised using standard Olink workflows to produce relative protein abundance on a log2 scale ('NPX'). BAL and plasma proteomic data were normalised separately. Quality assessment was performed by (1) examination of Olink internal controls and (2) inspection of boxplots, relative log expression plots, and PCA. PCA was performed using singular value decomposition. Following these steps, 2 clear outlying samples were removed from the BAL dataset. To identify proteins that were differentially abundant between case and controls, for each protein we performed linear regression (lm function in R) with case/control status as the independent variable and protein concentration (NPX/ml) as the dependent variable. P-values were adjusted for multiple testing using the Benjamini-Hochberg procedure (p.adjust function in R). A 5% false discovery rate was used to define statistical significance. We used the WGCNA R package (Langfelder and Horvath, 2008; Zhang and Horvath, 2005) to create a weighted protein correlation network. Prior to WGCNA analysis, protein data were scaled and centred, and missing data were imputed using the R caret package. We used the WCGNA adjacency function to produce a weighed network adjacency matrix, using parameters "type=signed" and "power=13". This soft-thresholding power was selected as the lowest power to achieve approximate scale-free topology. We next defined a topological overlap matrix of dissimilarity using the TOMdist function. Clusters ('modules') of interconnected proteins were identified using hierarchical clustering and the cutreeDynamic function with parameters: method="hybrid", deepSplit=2, minClusterSize=15. We then tested association of these modules with case/control status. Multiple testing correction was performed to account for the number of modules. We report both Benjamini-Hochberg and Bonferroni adjusted p-values to provide two levels of stringency. To assess the distribution of p-values from the differential protein abundance analyses, we plotted histograms and constructed QQ plots. QQ plots were made by comparing the expected distribution of -log10 P values under the null hypothesis of no proteomic differences between post-COVID19 patients and controls to the observed p-values for the 435 proteins. We performed

pathway enrichment analysis for the 435 proteins measured. This was performed using terms from KEGG database (**Supplementary File 1B**) and the Reactome database (**Supplementary File 1C**). Protein modules were visualised using STRING (https://string-db.org/), with known or suspected interconnections between module members displayed as edges in a network diagram. An edge represents a protein-to-protein relationship defined as shared contributions to a particular function, and not necessarily implying physical binding. In **Figure 3C**, edge colour indicates the type of evidence for the relationship: turquoise represents known interactions from curated databases; magenta represents experimentally determined interactions; green represents predicted Interactions from gene neighbourhood analysis; red represent predicted interactions from gene fusions, blue represent predicted Interactions from gene co-occurrence; light green represents interaction from text-mining; black represents interaction from co-expression data, and violet represents information from protein homology.

Quantification and statistical analysis for flow cytometry and univariate assays
Differences in means between two sample groups were compared using two-tailed Mann-Whitney U tests. Multiple group comparisons were done using Kruskal Wallis ANOVA followed by Dunn's post-test. Spearman-Rank correlations immune cell versus clinical and biomarker traits. Analysis was performed in GraphPad Prism. For all figures, * denotes p value < 0.05, ** denotes p value < 0.01 and *** denotes p value < 0.001. Where multiple tests were carried out significance was assessed by carrying out a Benjamini-Hochberg set to 5% FDR.

Summary diagrams. The summary schematic and graphical abstract were designed using BioRender.

Supplemental data

Supplemental table 2 post-COVID19 proteomics analysis. Related to figure 3. A spreadsheet (tables A-L) detail statistical analysis of post-COVID19 BAL and plasma proteomes. DOI: 10.17632/th35tt4zwm.1

References

Ali, M.F., Egan, A.M., Shaughnessy, G.F., Anderson, D.K., Kottom, T.J., Dasari, H., Van Keulen, V.P., Aubry, M.C., Yi, E.S., Limper, A.H.*, et al.* (2021). Antifibrotics Modify B-Cell-induced Fibroblast Migration and Activation in Patients with Idiopathic Pulmonary Fibrosis. Am J Respir Cell Mol Biol *64*, 722-733.

Allden, S.J., Ogger, P.P., Ghai, P., McErlean, P., Hewitt, R., Toshner, R., Walker, S.A., Saunders, P., Kingston, S., Molyneaux, P.L.*, et al.* (2019). The Transferrin Receptor CD71 Delineates Functionally Distinct Airway Macrophage Subsets during Idiopathic Pulmonary Fibrosis. Am J Respir Crit Care Med *200*, 209-219.

Arunachalam, P.S., Wimmers, F., Mok, C.K.P., Perera, R., Scott, M., Hagan, T., Sigal, N., Feng, Y., Bristow, L., Tak-Yin Tsang, O.*, et al.* (2020). Systems biological assessment of immunity to mild versus severe COVID-19 infection in humans. Science *369*, 1210-1220.

Asai, Y., Chiba, H., Nishikiori, H., Kamekura, R., Yabe, H., Kondo, S., Miyajima, S., Shigehara, K., Ichimiya, S., and Takahashi, H. (2019). Aberrant populations of circulating T follicular helper cells and regulatory B cells underlying idiopathic pulmonary fibrosis. Respir Res *20*, 244.

Boyd, D.F., Allen, E.K., Randolph, A.G., Guo, X.J., Weng, Y., Sanders, C.J., Bajracharya, R., Lee, N.K., Guy, C.S., Vogel, P.*, et al.* (2020). Exuberant fibroblast activity compromises lung function via ADAMTS4. Nature *587*, 466-471.

Byrne, A.J., Powell, J.E., O'Sullivan, B.J., Ogger, P.P., Hoffland, A., Cook, J., Bonner, K.L., Hewitt, R.J., Wolf, S., Ghai, P.*, et al.* (2020). Dynamics of human monocytes and airway macrophages during healthy aging and after transplant. J Exp Med *217*.

Chen, Z., and Wherry, E.J. (2020). T cell responses in patients with COVID-19. Nat Rev Immunol *20*, 529-536.

Cheon, I.S., Li, C., Son, Y.M., Goplen, N.P., Wu, Y., Cassmann, T., Wang, Z., Wei, X., Tang, J., Li, Y.*, et al.* (2021). Immune signatures underlying post-acute COVID-19 lung sequelae. Sci Immunol, eabk1741.

Dan, J.M., Mateus, J., Kato, Y., Hastie, K.M., Yu, E.D., Faliti, C.E., Grifoni, A., Ramirez, S.I., Haupt, S., Frazier, A.*, et al.* (2021). Immunological memory to SARS-CoV-2 assessed for up to 8 months after infection. Science *371*.

Desai, O., Winkler, J., Minasyan, M., and Herzog, E.L. (2018). The Role of Immune and Inflammatory Cells in Idiopathic Pulmonary Fibrosis. Front Med (Lausanne) *5*, 43.

Docherty, A.B., Harrison, E.M., Green, C.A., Hardwick, H.E., Pius, R., Norman, L., Holden, K.A., Read, J.M., Dondelinger, F., Carson, G.*, et al.* (2020). Features of 20 133 UK patients in hospital with covid-19 using the ISARIC WHO Clinical Characterisation Protocol: prospective observational cohort study. BMJ *369*, m1985.

Drake, T.M., Riad, A.M., Fairfield, C.J., Egan, C., Knight, S.R., Pius, R., Hardwick, H.E., Norman, L., Shaw, C.A., McLean, K.A.*, et al.* (2021). Characterisation of in-hospital complications associated with COVID-19 using the ISARIC WHO Clinical Characterisation Protocol UK: a prospective, multicentre cohort study. Lancet *398*, 223-237.

Duan, S., and Thomas, P.G. (2016). Balancing Immune Protection and Immune Pathology by CD8(+) T-Cell Responses to Influenza Infection. Front Immunol *7*, 25.

Evren, E., Ringqvist, E., Tripathi, K.P., Sleiers, N., Rives, I.C., Alisjahbana, A., Gao, Y., Sarhan, D., Halle, T., Sorini, C.*, et al.* (2021). Distinct developmental pathways from blood monocytes generate human lung macrophage diversity. Immunity *54*, 259-275 e257.

Fabbri, L., Moss, S., Khan, F., Chi, W., Xia, J., Robinson, K., Smyth, A., Jenkins, G., and Stewart, I. (2021). Post-viral parenchymal lung disease of COVID-19 and viral pneumonitis: A systematic review and meta-analysis. medRxiv, 2021.2003.2015.21253593.

Filbin, M.R., Mehta, A., Schneider, A.M., Kays, K.R., Guess, J.R., Gentili, M., Fenyves, B.G., Charland, N.C., Gonye, A.L.K., Gushterova, I.*, et al.* (2021). Longitudinal

proteomic analysis of severe COVID-19 reveals survival-associated signatures, tissue-specific cell death, and cell-cell interactions. Cell Rep Med *2*, 100287.

Gisby, J., Clarke, C.L., Medjeral-Thomas, N., Malik, T.H., Papadaki, A., Mortimer, P.M., Buang, N.B., Lewis, S., Pereira, M., Toulza, F.*, et al.* (2021). Longitudinal proteomic profiling of dialysis patients with COVID-19 reveals markers of severity and predictors of death. Elife *10*.

Grau-Exposito, J., Sanchez-Gaona, N., Massana, N., Suppi, M., Astorga-Gamaza, A., Perea, D., Rosado, J., Falco, A., Kirkegaard, C., Torrella, A.*, et al.* (2021). Peripheral and lung resident memory T cell responses against SARS-CoV-2. Nat Commun *12*, 3010.

Guler, S.A., Ebner, L., Aubry-Beigelman, C., Bridevaux, P.O., Brutsche, M., Clarenbach, C., Garzoni, C., Geiser, T.K., Lenoir, A., Mancinetti, M.*, et al.* (2021). Pulmonary function and radiological features 4 months after COVID-19: first results from the national prospective observational Swiss COVID-19 lung study. Eur Respir J *57*.

Han, X., Fan, Y., Alwalid, O., Li, N., Jia, X., Yuan, M., Li, Y., Cao, Y., Gu, J., Wu, H., and Shi, H. (2021). Six-month Follow-up Chest CT Findings after Severe COVID-19 Pneumonia. Radiology *299*, E177-E186.

Harker, J.A., and Lloyd, C.M. (2021). Overlapping and distinct features of viral and allergen immunity in the human lung. Immunity *54*, 617-631.

Invernizzi, R., Wu, B.G., Barnett, J., Ghai, P., Kingston, S., Hewitt, R.J., Feary, J., Li, Y., Chua, F., Wu, Z.*, et al.* (2021). The Respiratory Microbiome in Chronic Hypersensitivity Pneumonitis Is Distinct from That of Idiopathic Pulmonary Fibrosis. Am J Respir Crit Care Med *203*, 339-347.

Jozwik, A., Habibi, M.S., Paras, A., Zhu, J., Guvenel, A., Dhariwal, J., Almond, M., Wong, E.H.C., Sykes, A., Maybeno, M.*, et al.* (2015). RSV-specific airway resident memory CD8+ T cells and differential disease severity after experimental human infection. Nat Commun *6*, 10224.

Kim, T.S., Hufford, M.M., Sun, J., Fu, Y.X., and Braciale, T.J. (2010). Antigen persistence and the control of local T cell memory by migrant respiratory dendritic cells after acute virus infection. J Exp Med *207*, 1161-1172.

Kory, P., and Kanne, J.P. (2020). SARS-CoV-2 organising pneumonia: 'Has there been a widespread failure to identify and treat this prevalent condition in COVID-19?'. BMJ Open Respir Res *7*.

Laing, A.G., Lorenc, A., Del Molino Del Barrio, I., Das, A., Fish, M., Monin, L., Munoz-Ruiz, M., McKenzie, D.R., Hayday, T.S., Francos-Quijorna, I.*, et al.* (2020). A dynamic COVID-19 immune signature includes associations with poor prognosis. Nat Med *26*, 1623-1635.

Langfelder, P., and Horvath, S. (2008). WGCNA: an R package for weighted correlation network analysis. BMC Bioinformatics *9*, 559.

Li, Y., Zhang, Z., Yang, L., Lian, X., Xie, Y., Li, S., Xin, S., Cao, P., and Lu, J. (2020). The MERS-CoV Receptor DPP4 as a Candidate Binding Target of the SARS-CoV-2 Spike. iScience *23*, 101400.

Liao, M., Liu, Y., Yuan, J., Wen, Y., Xu, G., Zhao, J., Cheng, L., Li, J., Wang, X., Wang, F.*, et al.* (2020). Single-cell landscape of bronchoalveolar immune cells in patients with COVID-19. Nat Med *26*, 842-844.

Lucas, C., Wong, P., Klein, J., Castro, T.B.R., Silva, J., Sundaram, M., Ellingson, M.K., Mao, T., Oh, J.E., Israelow, B.*, et al.* (2020). Longitudinal analyses reveal immunological misfiring in severe COVID-19. Nature *584*, 463-469.

Mandal, S., Barnett, J., Brill, S.E., Brown, J.S., Denneny, E.K., Hare, S.S., Heightman, M., Hillman, T.E., Jacob, J., Jarvis, H.C.*, et al.* (2021). 'Long-COVID': a cross-sectional study of persisting symptoms, biomarker and imaging abnormalities following hospitalisation for COVID-19. Thorax *76*, 396-398.

Mann, E.R., Menon, M., Knight, S.B., Konkel, J.E., Jagger, C., Shaw, T.N., Krishnan, S., Rattray, M., Ustianowski, A., Bakerly, N.D*., et al.* (2020). Longitudinal immune profiling reveals key myeloid signatures associated with COVID-19. Sci Immunol *5*.
Misharin, A.V., Morales-Nebreda, L., Reyfman, P.A., Cuda, C.M., Walter, J.M., McQuattie-Pimentel, A.C., Chen, C.I., Anekalla, K.R., Joshi, N., Williams, K.J.N*., et al.* (2017). Monocyte-derived alveolar macrophages drive lung fibrosis and persist in the lung over the life span. J Exp Med *214*, 2387-2404.
Morimoto, Y., Hirahara, K., Kiuchi, M., Wada, T., Ichikawa, T., Kanno, T., Okano, M., Kokubo, K., Onodera, A., Sakurai, D*., et al.* (2018). Amphiregulin-Producing Pathogenic Memory T Helper 2 Cells Instruct Eosinophils to Secrete Osteopontin and Facilitate Airway Fibrosis. Immunity *49*, 134-150 e136.
Myall, K.J., Mukherjee, B., Castanheira, A.M., Lam, J.L., Benedetti, G., Mak, S.M., Preston, R., Thillai, M., Dewar, A., Molyneaux, P.L., and West, A.G. (2021). Persistent Post-COVID-19 Interstitial Lung Disease. An Observational Study of Corticosteroid Treatment. Ann Am Thorac Soc *18*, 799-806.
Nalbandian, A., Sehgal, K., Gupta, A., Madhavan, M.V., McGroder, C., Stevens, J.S., Cook, J.R., Nordvig, A.S., Shalev, D., Sehrawat, T.S*., et al.* (2021). Post-acute COVID-19 syndrome. Nat Med *27*, 601-615.
Polverino, F., Seys, L.J., Bracke, K.R., and Owen, C.A. (2016). B cells in chronic obstructive pulmonary disease: moving to center stage. Am J Physiol Lung Cell Mol Physiol *311*, L687-L695.
Poon, M.M.L., Rybkina, K., Kato, Y., Kubota, M., Matsumoto, R., Bloom, N.I., Zhang, Z., Hastie, K.M., Grifoni, A., Weiskopf, D*., et al.* (2021). SARS-CoV-2 infection generates tissue-localized immunological memory in humans. Sci Immunol, eabl9105.
Pribul, P.K., Harker, J., Wang, B., Wang, H., Tregoning, J.S., Schwarze, J., and Openshaw, P.J. (2008). Alveolar macrophages are a major determinant of early responses to viral lung infection but do not influence subsequent disease development. J Virol *82*, 4441-4448.
Raj, V.S., Mou, H., Smits, S.L., Dekkers, D.H., Muller, M.A., Dijkman, R., Muth, D., Demmers, J.A., Zaki, A., Fouchier, R.A*., et al.* (2013). Dipeptidyl peptidase 4 is a functional receptor for the emerging human coronavirus-EMC. Nature *495*, 251-254.
Rodriguez, L., Pekkarinen, P.T., Lakshmikanth, T., Tan, Z., Consiglio, C.R., Pou, C., Chen, Y., Mugabo, C.H., Nguyen, N.A., Nowlan, K*., et al.* (2020). Systems-Level Immunomonitoring from Acute to Recovery Phase of Severe COVID-19. Cell Rep Med *1*, 100078.
Saris, A., Reijnders, T.D.Y., Nossent, E.J., Schuurman, A.R., Verhoeff, J., Asten, S.V., Bontkes, H., Blok, S., Duitman, J., Bogaard, H.J*., et al.* (2021). Distinct cellular immune profiles in the airways and blood of critically ill patients with COVID-19. Thorax.
Schmidt, M.E., and Varga, S.M. (2018). The CD8 T Cell Response to Respiratory Virus Infections. Front Immunol *9*, 678.
Scott, N.A., Knight, S.B., Pearmain, L., Brand, O., Morgan, D.J., Jagger, C., Khan, S., Hackney, P., Smith, L., Menon, M*., et al.* (2020). Recovery of monocyte exhaustion is associated with resolution of lung injury in COVID-19 convalescence. medRxiv, 2020.2010.2010.20207449.
Sigfrid, L., Drake, T.M., Pauley, E., Jesudason, E.C., Olliaro, P., Lim, W.S., Gillesen, A., Berry, C., Lowe, D.J., McPeake, J*., et al.* (2021). Long Covid in adults discharged from UK hospitals after Covid-19: A prospective, multicentre cohort study using the ISARIC WHO Clinical Characterisation Protocol. medRxiv, 2021.2003.2018.21253888.
Slutter, B., Pewe, L.L., Kaech, S.M., and Harty, J.T. (2013). Lung airway-surveilling CXCR3(hi) memory CD8(+) T cells are critical for protection against influenza A virus. Immunity *39*, 939-948.
Slutter, B., Van Braeckel-Budimir, N., Abboud, G., Varga, S.M., Salek-Ardakani, S., and Harty, J.T. (2017). Dynamics of influenza-induced lung-resident memory T cells underlie waning heterosubtypic immunity. Sci Immunol *2*.

Szabo, P.A., Dogra, P., Gray, J.I., Wells, S.B., Connors, T.J., Weisberg, S.P., Krupska, I., Matsumoto, R., Poon, M.M.L., Idzikowski, E.*, et al.* (2021). Longitudinal profiling of respiratory and systemic immune responses reveals myeloid cell-driven lung inflammation in severe COVID-19. Immunity *54*, 797-814 e796.

Szabo, P.A., Miron, M., and Farber, D.L. (2019). Location, location, location: Tissue resident memory T cells in mice and humans. Sci Immunol *4*.

Thwaites, R.S., Sanchez Sevilla Uruchurtu, A., Siggins, M.K., Liew, F., Russell, C.D., Moore, S.C., Fairfield, C., Carter, E., Abrams, S., Short, C.E.*, et al.* (2021). Inflammatory profiles across the spectrum of disease reveal a distinct role for GM-CSF in severe COVID-19. Sci Immunol *6*.

Vijayakumar, B., Tonkin, J., Devaraj, A., Philip, K.E.J., Orton, C.M., Desai, S.R., and Shah, P.L. (2021). CT Lung Abnormalities after COVID-19 at 3 Months and 1 Year after Hospital Discharge. Radiology, 211746.

Wang, E.Y., Mao, T., Klein, J., Dai, Y., Huck, J.D., Liu, F., Zheng, N.S., Zhou, T., Israelow, B., Wong, P.*, et al.* (2020). Diverse Functional Autoantibodies in Patients with COVID-19. medRxiv, 2020.2012.2010.20247205.

Wu, T., Hu, Y., Lee, Y.T., Bouchard, K.R., Benechet, A., Khanna, K., and Cauley, L.S. (2014). Lung-resident memory CD8 T cells (TRM) are indispensable for optimal cross-protection against pulmonary virus infection. J Leukoc Biol *95*, 215-224.

Yamashita, C.M., Dolgonos, L., Zemans, R.L., Young, S.K., Robertson, J., Briones, N., Suzuki, T., Campbell, M.N., Gauldie, J., Radisky, D.C.*, et al.* (2011). Matrix metalloproteinase 3 is a mediator of pulmonary fibrosis. Am J Pathol *179*, 1733-1745.

Zhang, B., and Horvath, S. (2005). A general framework for weighted gene co-expression network analysis. Stat Appl Genet Mol Biol *4*, Article17.

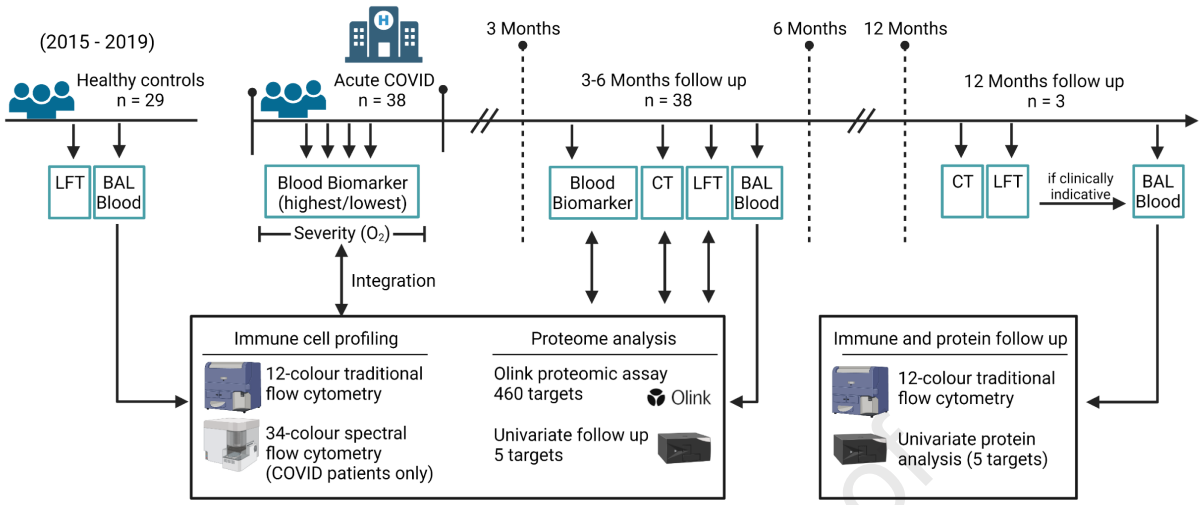

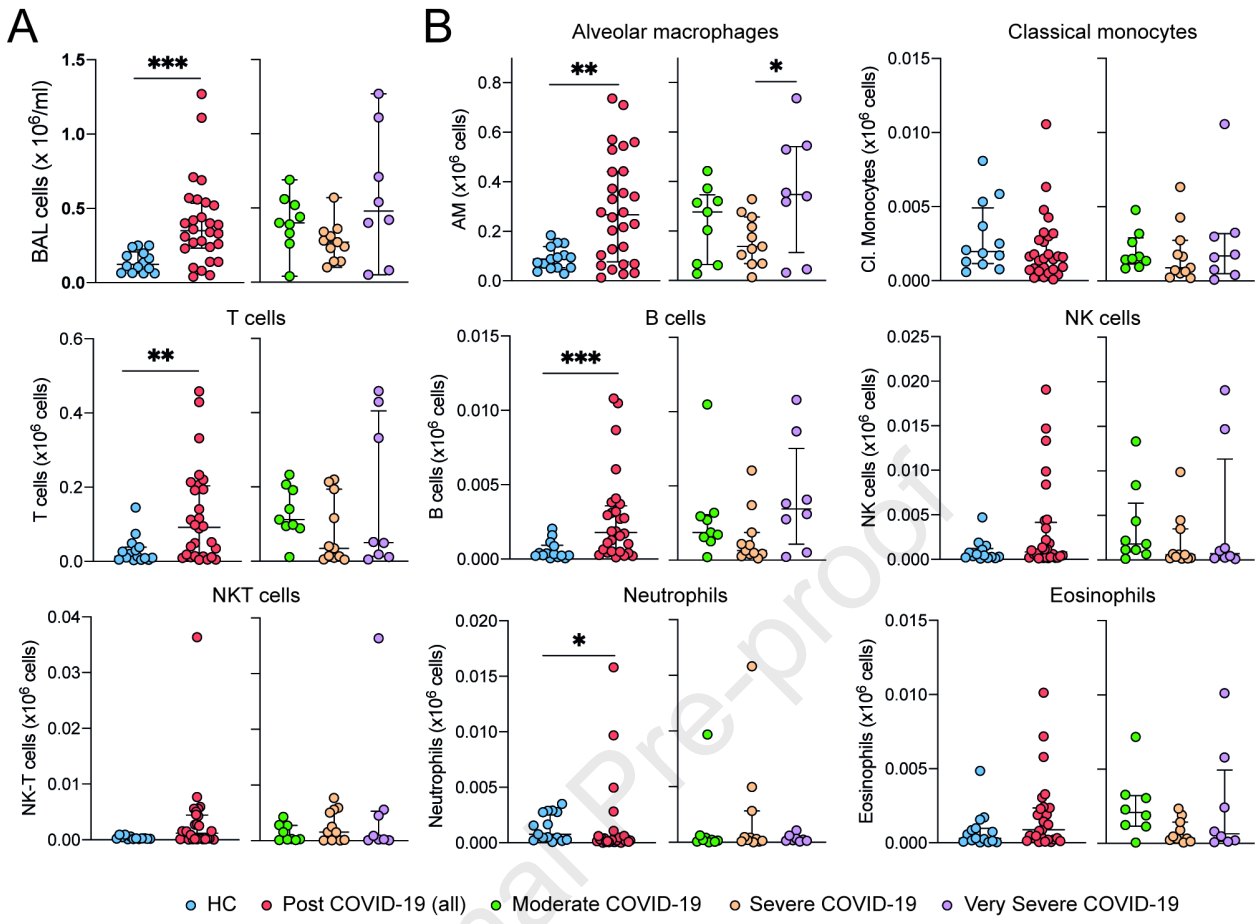

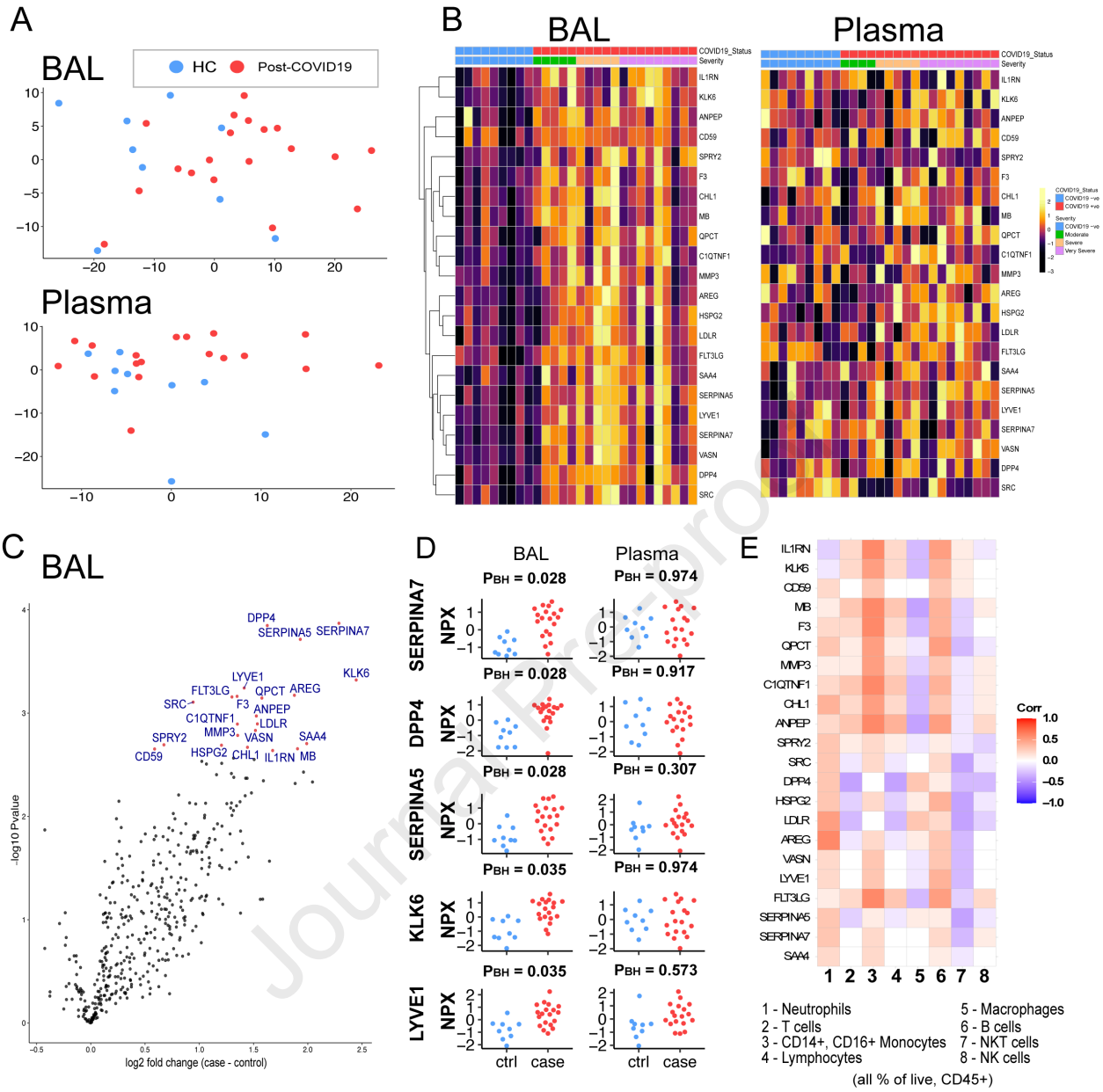

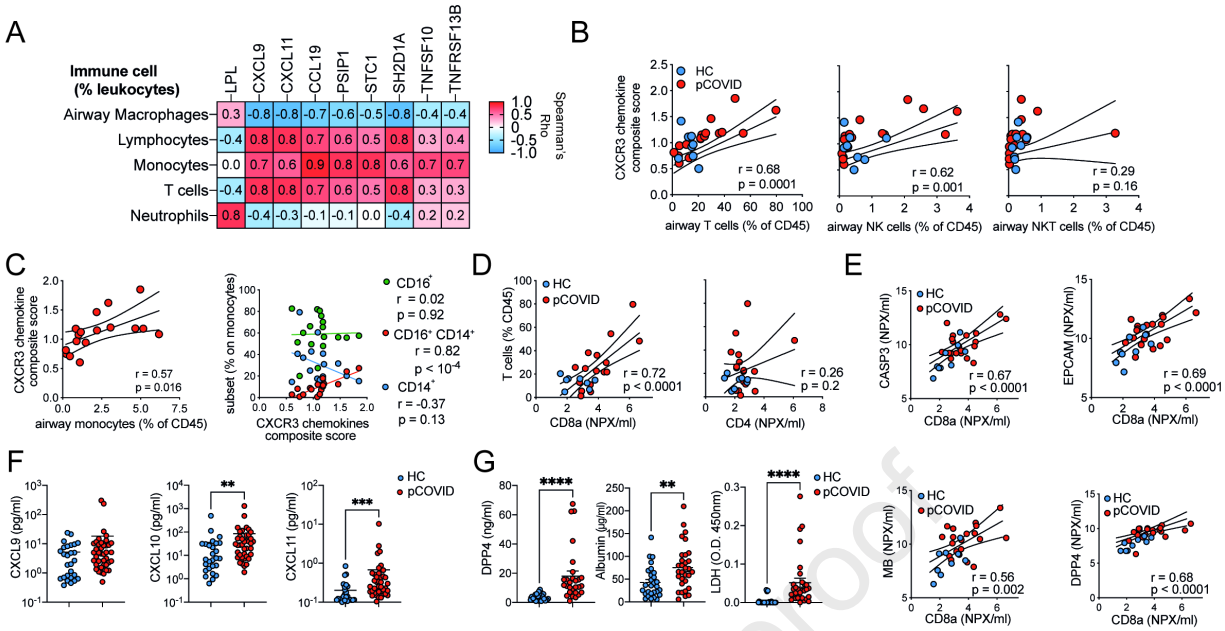

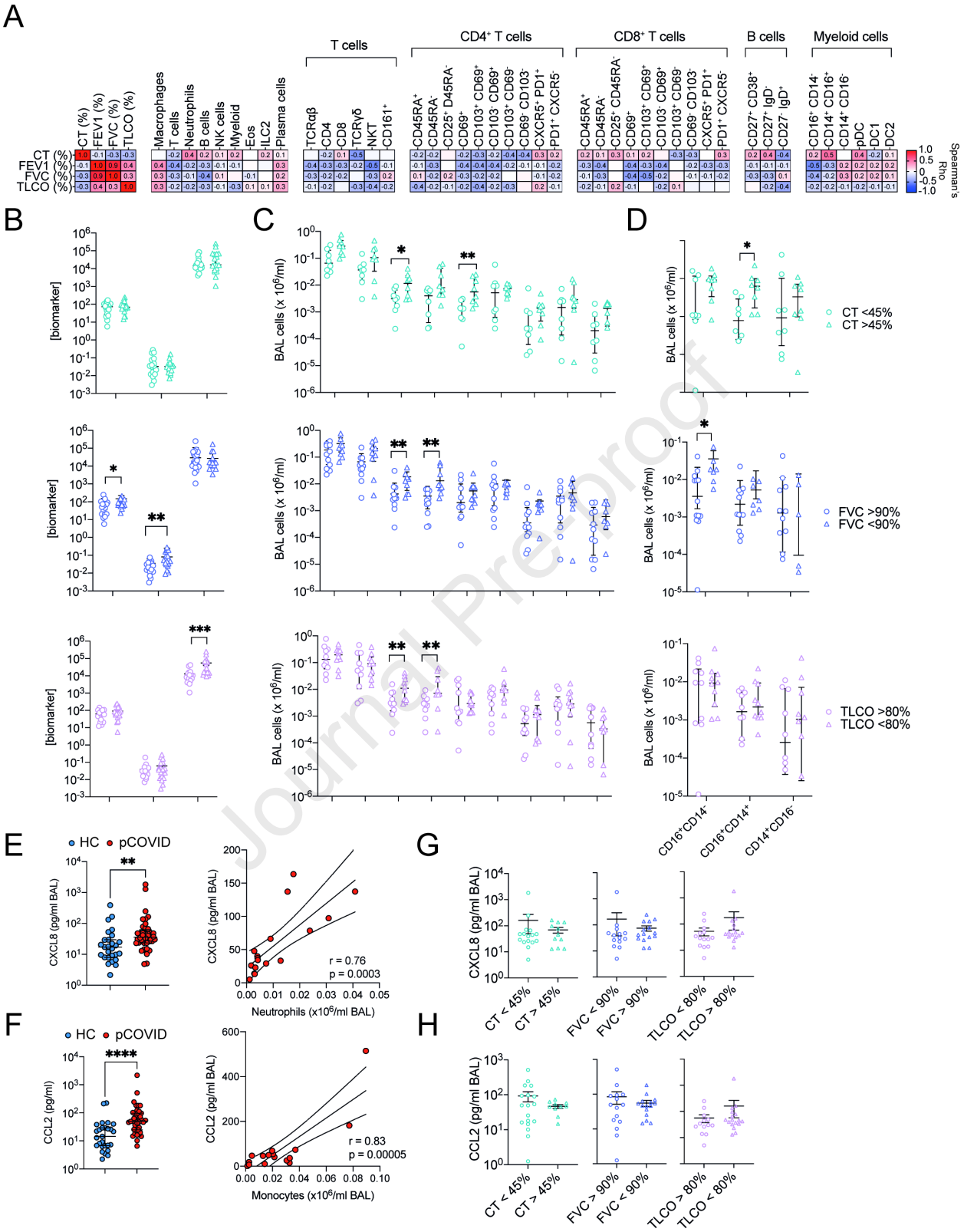

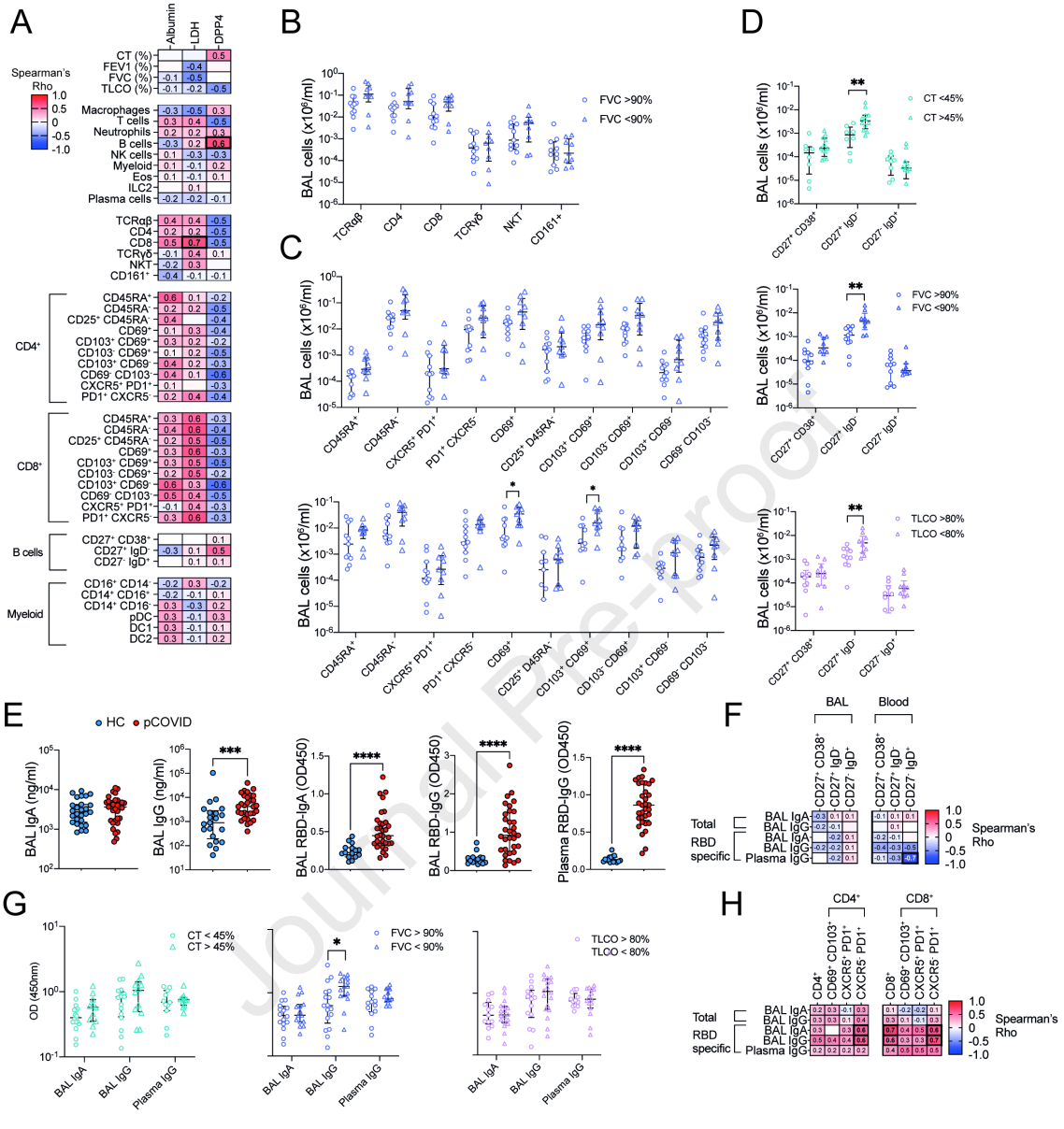

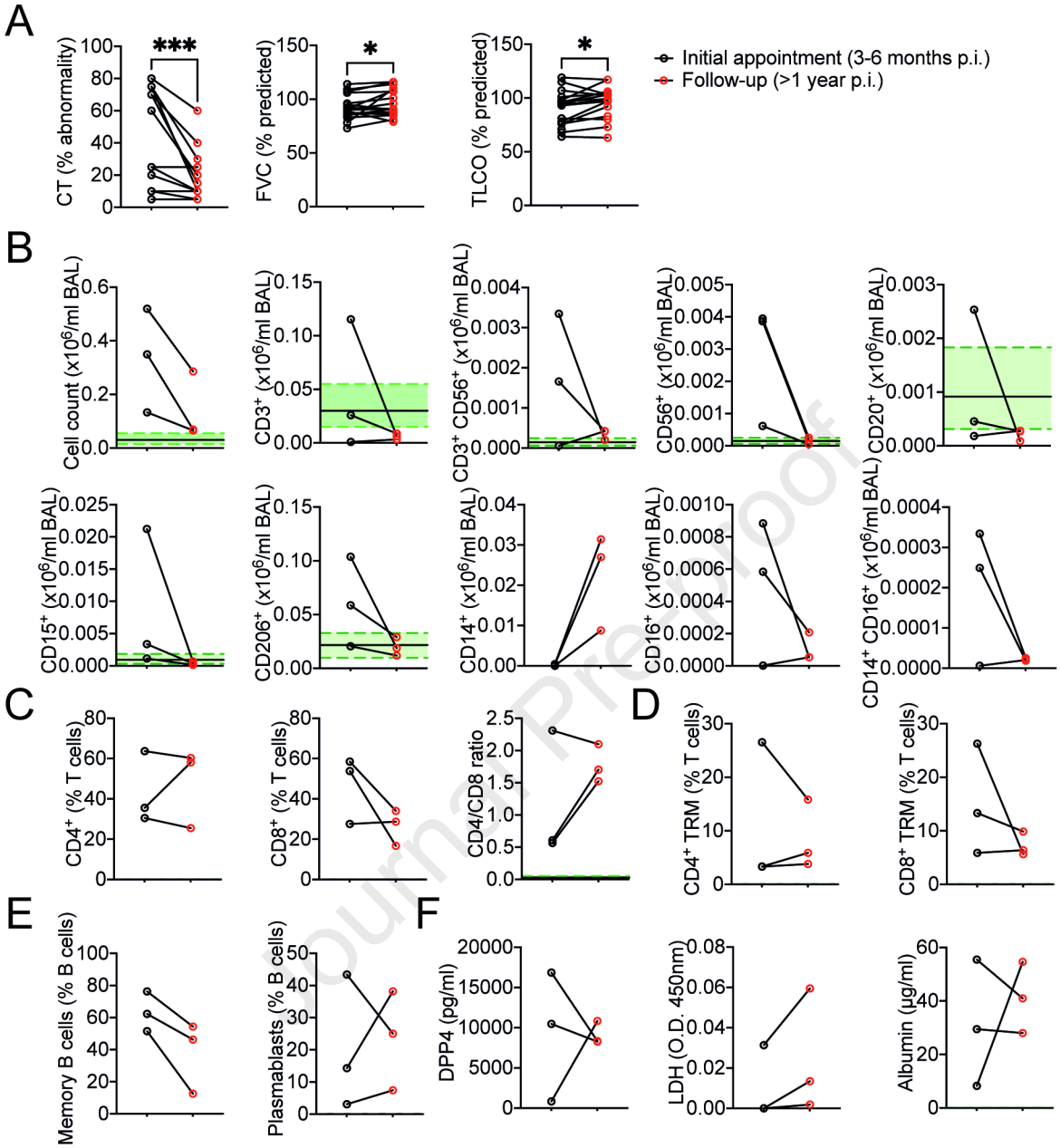

Highlights

- Post-COVID19 airways, but not blood, show T cells, B cells macrophages and proteomic changes.
- Different post-COVID19 lung abnormalities relate to distinct immunological features.
- Increased BAL cytotoxic T cells are linked to epithelial damage and airways disease.
- BAL myeloid and B cell numbers correlate with the degree of lung CT abnormality.

eTOC

Many individuals recovering from acute SARS-CoV-2 infection suffer prolonged respiratory dysfunction for months to years after viral clearance. Vijayakumar, Boustani, Ogger, Papadaki et al. show that individuals with persistent symptoms 3-6 months after infection have an altered airway immune cell landscape and evidence of ongoing lung damage. Importantly, different immune cell types correlate with the severity of distinct aspects of ongoing respiratory disease.

Key resources table

REAGENT or RESOURCE	SOURCE	IDENTIFIER
Antibodies		
Anti-Human CD69, BUV395	BD Biosciences	Cat#564364
Anti-human CD8, BUV496	BD Biosciences	Cat#612942
Anti-Human CD45RA, BUV563	BD Biosciences	Cat#612927
Anti-Human CD11c, BUV661	BD Biosciences	Cat#612968
Anti-Human CD56, BUV737	BD Biosciences	Cat#612767
Anti-Human CD3, BUV805	BD Biosciences	Cat#612896
Anti-Human IgD, BV421	Biolegend	Cat#348226
Anti-Human CD16, SuperBright436	ThermoFisher	Cat#62-0166-42
Anti-Human CD25, eFluor450	ThermoFisher	Cat#48-0257-42
Anti-Human CD20, BV480	BD Biosciences	Cat#566132
Anti-Human CD127, BV510	Biolegend	Cat#351332
Anti-Human HLA-DR, BV570	Biolegend	Cat#307638
Anti-Human CD28, BV605	Biolegend	Cat#302968
Anti-Human CD38, BV650	Biolegend	Cat#356620
Anti-Human CD15, BV711	Biolgend	Cat#323050
Anti-Human CD279, BV750	Biolegend	Cat#329966
Anti-Human CD206, BV785	Biolegend	Cat#321142
Anti-Human CD45, QDOT800	ThermoFisher	Cat#Q10156
Anti-Human CXCR5, BB515	BD Biosciences	Cat#564624
Anti-Human CD169, AF488	R&D systems	Cat#FAB5197G
Anti-Human CD4, Spark Blue 550	Biolegend	Cat#344656
Anti-Human CD161, PerCP	Biolegend	Cat#3399334
Anti-Human CD27, BB700	BD Biosciences	Cat#566449
Anti-Human Siglec8, PerCP Cy5.5	Biolegend	Cat#347108
Anti-Human CD86, PerC eFLuor710	ThermoFisher	Cat#46-0869-42
Anti-Human CD141, PE	Biolegend	Cat#344104
Anti-Human TCRg/d, PEdz594	Biolegend	Cat#331226
Anti-Human TCRa/b PE Cy5	Biolegend	Cat#306710
Anti-Human CD11b, PE Cy7	Biolegend	Cat#301322
Anti-Human CD123, APC	Biolegend	Cat#306012
Anti-Human CRTH2, AF647	Biolegend	Cat#350104
Anti-Human CD14, Spark NIR	Biolegend	Cat#367150
Anti-Human CD1c, APC R700	BD Biosciences	Cat#566614
Anti-Human CD103, APC Cy7	Biolegend	Cat#350228
Anti-Human CD45, PerCP Cy5.5	ThermoFisher	Cat#45-0459-42
Anti-Human Siglec8, AF488	R&D systems	Cat#FAB7975G
Anti-Human CD19, BV421	Biolegend	Cat#302234
Anti-Human CD4, BV510	Biolegend	Cat#317444
Anti-Human CD117, BV605	Biolegend	Cat#313218
Anti-Human CD14, BV711	Biolegend	Cat#301838
Anti-Human CD16, BV785	Biolegend	Cat#302046
Anti-Human CD177, FITC	Biolegend	Cat#315804
Anti-Human Siglec8, PE	R&D systems	Cat#FAB7975P
Anti-Human CD56, PEdz594	Biolegend	Cat#318348
Anti-Human CD3, PE-Cy7	Biolegend	Cat#300420

Anti-Human CD206, APC	Biolegend	Cat#321110
Anti-Human FcE, AF700	Biolegend	Cat#334630
Chemicals, peptides, and recombinant proteins		
LIVE/DEAD Fixable NIR Cell Stain	ThermoFisher	Cat#L34976
LIVE/DEAD Fixable Blue? Cell Stain	ThermoFisher	Cat#L34961
TruStain FcX	Biolegend	Cat#422302
RPMI 1640	Gibco	Cat#21875091
Critical commercial assays		
Target 96 Cardiometabolic Assay	Olink	Cat#91802
Target 96 CVD II Assay	Olink	Cat#91202
Target 96 CVD III Assay	Olink	Cat#91203
Target 96 Immune Response Assay	Olink	Cat#91701
Target 96 Inflammation Assay	Olink	Cat#91301
DPP4 ELISA	R&D Systems	Cat#DY1180
Albumin ELISA	Bethyl Laboratories	Cat#E80-129
LDH Assay	Sigma Aldrich	Cat#TOX7
LEGENDplex Human Proinflam. Chemokine Panel 1	Biolegend	Cat#740984
Deposited data		
Proteomic data and associated clinical and demographic information	Dryad	https://doi.org/10.5061/dryad.2ngf1vhq3
R code used in analysis of proteomic data	Github/Zenodo	https://doi.org/10.5281/zenodo.5844957
Software and algorithms		
Flowjo version 10.7 software	Treestar	https://www.flowjo.com
STRING protein module visualisation	String	https://www.string-db.org
RStudio version 1.2.1335	RStudio (2019)	https://www.rstudio.com
R version 3.5	R Foundation for Statistical Computing (2017)	https://www.R-project.org